A MICROSCOPIC MODEL FOR MICROTUBULES

By

MITHUN KUMAR MITRA

A Thesis Submitted to the

FACULTY OF SCIENCE AND HUMANITIES

in partial fulfilment of the requirements
for the award of the degree of

MASTER OF SCIENCE
(by Research)
in
THEORETICAL PHYSICS

ANNA UNIVERSITY
CHENNAI 600 025
March 2004

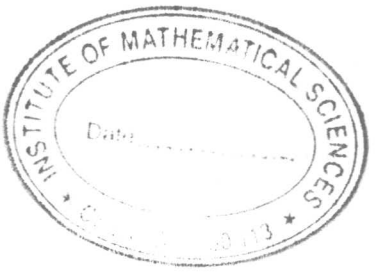

BONAFIDE CERTIFICATE

Certified that this dissertation titled **A MICROSCOPIC MODEL FOR MICROTUBULES** is the bonafide work of **Mr. MITHUN KUMAR MITRA** who carried out the project under my supervision. Certified further, that to the best of my knowledge the work reported herein does not form part of any other dissertation on the basis of which a degree or award was conferred on an earlier occasion on this or any other candidate.

Prof. R.D. Rajan
Head, Department of Physics
Anna University

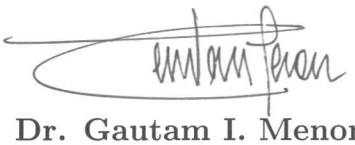

Dr. Gautam I. Menon
Theoretical Physics
Institute of Mathematical Sciences
Chennai

March 2004

Abstract

An important class of force generating mechanisms in living cells involves the controlled polymerization and depolymerization of biological macromolecules, such as Microtubules. There has been much activity in trying to understand the mechanism by which a microtubule alternates between polymerization and depolymerization. While several interesting hypotheses have been made over the last decade or so, progress has been slow due to the absence of a microscopic model which can properly explain the various observed properties of the microtubule.

In this thesis we try to constuct a microscopic model for the microtubule which can reproduce the experimentally observed structures. The basic subunit of our model is the tubulin heterodimer, and we construct the microtubule by arranging 13 protofilaments in a cylindrical lattice. Each subunit of the microtubule lattice is connected to its four nearest neighbours by springs, and the energetics penalises deviations from the equilibrium bond length or the equilibrium bond angle both in the horizontal and vertical directions. There is also an energy cost for deviations from the perfect square topology between the bonds. In addition, we incorporate a self-avoiding energy term for the lateral and longitudinal bonds.

Having defined our model, firstly we study the elastic response of our model to small deformations. Specifically, we determine the torsional and tilt moduli of our model microtubule. We also study the equilibrium structures generated by Monte-Carlo and Brownian Dynamics simulations in different regimes of the parameters of our model both at zero and at finite temperatures. Finally, we try to provide a future direction for further work that needs to be done within the scope of the model.

பணிச்சுருக்கம்

உயிர் மேக்ரோ-மூலக்கூறுகளின் கட்டுப்படுத்தப்பட்ட பாலிமரிசேசனும், டிபாலிமரிசேசனும் உயிர் செல்களின் ஆற்றல் உருவாக்கும் பணிகளில் முக்கியப் பங்காற்றுகின்றன. மைக்ரோடுபியுல் எந்த வழிமுறையில், பாலிமரிசேசன், டிபாலிமரிசேசன் என்ற இரு மாறுபட்ட முறைகளை, மேற்கொள்கிறது என்பதைப் பற்றி அறிய பல ஆய்வுகள் மேற்கொள்ளப்பட்டுள்ளன. சென்ற பத்தாண்டுகளில் பல்வேறு கருத்து ஊகங்கள் இத்துறையில் சொல்லப்பட்டாலும் குறிப்பிட்த்தக்க முன்னேற்றம் எதுவும் இல்லை. மைக்ரோடுபியுலின் தன்மையை விளக்கத்தகுந்த நுண்மாதிரி இல்லாத்தே இதற்கு முக்கிய காரணம் ஆகும்.

இந்த ஆய்வில், சோதனையில் காணப்பட்ட கட்டமைப்பைத் தரக்கூடிய மைக்ரோடுபியுலின் முன்மாதிரியினைப் பெற முயல்கிறோம். நமது மாதிரியின் அடிப்படைத் துணை அலகு டுபியுலின்-ஹிடிரோடைமர் ஆகும். 13 புறொட்டோ-பிளமெண்டுகளை உருளைவடிவ லேடிஸில் வடிவமைப்பதன் மூலம் நாம் மைக்ரோடுபியுலைப் பெறுவோம். மைக்ரோடுபியுல் லேடிஸின் ஒவ்வொருத் துணை அலகும் அதன் மிக அருகில் உள்ள நான்கு துணை அலகுகலுடன் சுருள்கம்பிகளால் இணைக்கப்பட்டுள்ளது. எனர்ஜிடிக்ஸ் கிடைமட்ட மற்றும் செங்குத்துதிசைகளில் நிலைப்படுத்தப்பட்ட பிணைப்பின் நிளம் மற்றும் கோண மாறுபாடுகள் பெறப்படுகிறது. இந்த மாறுபாடுகளுக்கான ஆற்றல் இழப்பு சதுர டோபாலஜி கொண்டு அறியப்படுகிறது. துர மற்றும் உயர பிணைப்புகளுக்கான தான்-தவிர்ப்பு ஆற்றல் குணகம் பெறப்படுகிறது.

சுழி மற்றும் எந்த ஒரு குறிப்பிட்ட வெப்பநிலையிலும் நமது மாதிரியின் சமநிலைப்பட்ட கட்டமைப்பை மாண்டே-கார்லோ, புரோனியன் இயங்குவியல் முறையைப் பயன்படுத்தி அறிகிறோம். இறுதியாக வருங்காலத்தில் இந்த மாதிரியைக் கொண்டு மேற்கொள்ளக்கூடிய சாத்தியமான பணிகளைப் பற்றிய வரைவினைப் பெறுகிறோம்.

Acknowledgement

I am grateful to my parents and my sister for the love and support they have given to me throughout my life.

I sincerely thank my guide, Dr. Gautam I. Menon for the constant help and encouragement he has provided throughout this work.

I would like to thank all my friends for the help they have given me.

Special thanks are due to T. Muthukumar and R. Parthasarthi for their help in preparing this thesis.

Finally I must thank the institute and its academic and administrative members for providing an excellent academic atmosphere and facilities for research work.

Mithun Kumar Mitra

Contents

List of Tables

List of Figures

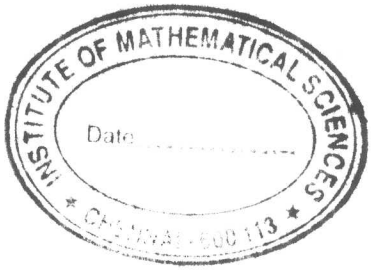

Chapter 1

INTRODUCTION

1.1 Microtubules

Cells are the basic components of all living organisms. To function properly, cells must be able to interact efficiently with their environment. Each cell must be able to handle a diverse array of spatial and mechanical functions for the organism to survive. The system of filaments which helps the cell in these functions is known as the cytoskeleton (Alberts et al., 2002).

In eucaryotic cells, there are three fundamental types of cytoskeletal filaments, microtubules, actin filaments, and intermediate filaments. Of these, in this thesis, we shall be concerned with microtubules only. Microtubules are responsible for various cell functions, including the beating of cilia and flagella, the formation of bundles that serve as tracks for the transport of materials in neuronal axons, and transport of membrane vesicles in the cytoplasm. Microtubules rearrange themselves to form the mitotic spindle during cell division and are also responsible for the arrangement and segregation of chromosomes during meiosis and mitosis. Microtubules also direct cell movement and can serve purely structural functions such as providing resilience to certain blood cells (Lodish et al., 1995).

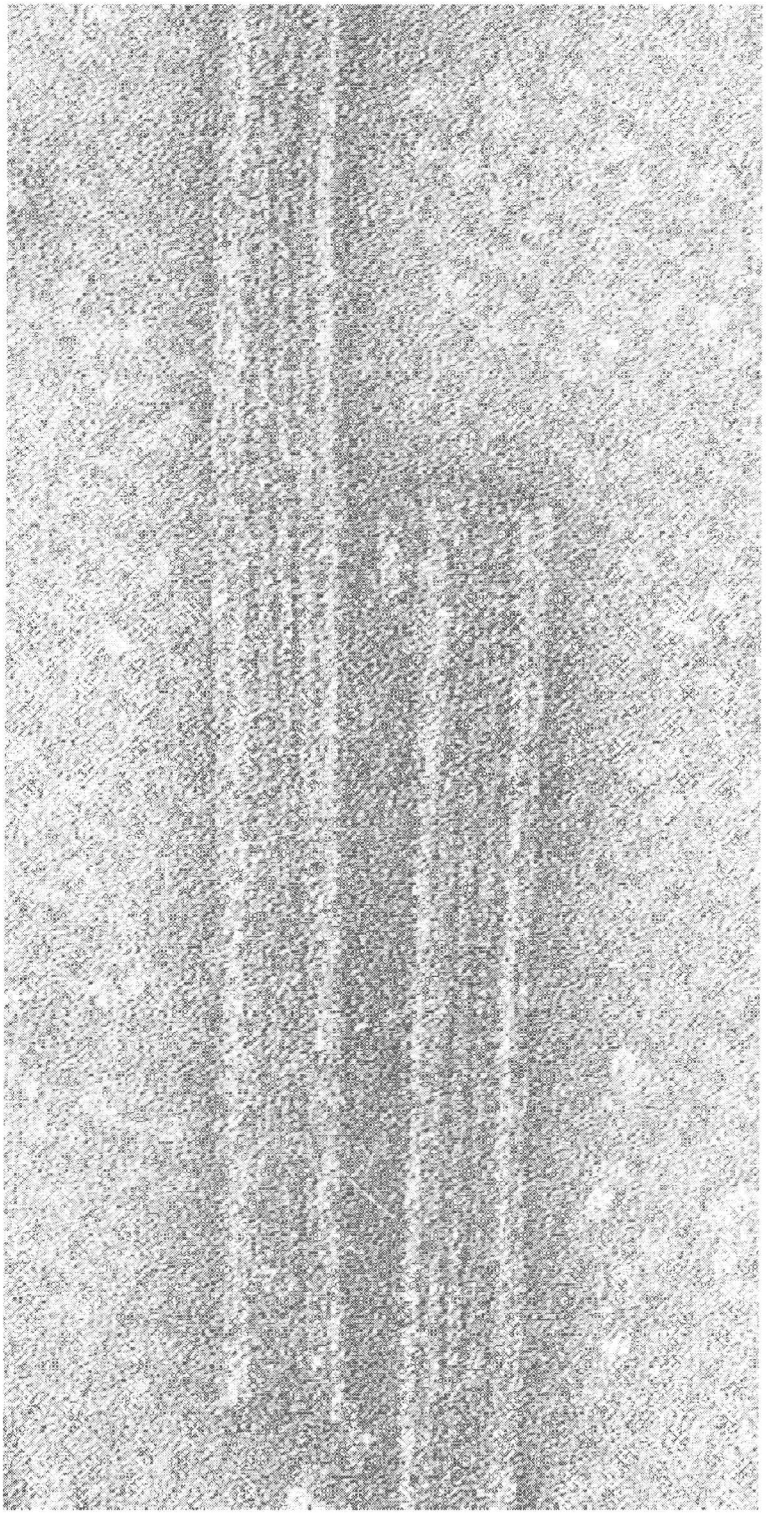

Figure 1.1: An electron micrograph picture of microtubule. (Reproduced from Lodish et.al. Chapter 23)

1.2 Structure of Microtubules

A microtubule(MT) is a polymer whose basic subunit is a tubulin heterodimer. The tubulin heterodimers are arranged in a cylindrical tube about 24 nm in diameter. The tubulin subunits arranged end-to-end form a structure known as the protofilament and the MT can then be thought of as being formed by these protofilaments arranged around a cylinder (Figure 1.2).

The basic subunit for a MT is the tubulin heterodimer which is composed of two globular proteins, the α and β tubulin monomers (Figure 1.3). Each tubulin monomer is a globular protein about 4 nm in diameter, and the heterodimer is thus 8 nm long. Each heterodimer binds two molecules of GTP (Guanosine Triphosphate) nucleotide, one each by the α and β monomers. The difference between the two subunits lies in their ability to hydrolyze this bound GTP molecule. The GTP-binding site located on the α-tubulin binds GTP irreversibly and does not hydrolyze it, whereas the GTP-binding site located on the β-tubulin binds GTP reversibly and hydrolyzes it to GDP. The second site, on the β-tubulin is known as the *exchangeable* site because GDP can be displaced by GTP. The interactions responsible for holding the α and β subunits together are very stable and the heterodimer cannot usually be broken up into its constituent monomers.

The tubular form of MTs is maintained by lateral and longitudinal interactions between the tubulin heterodimers. The longitudinal contacts between the heterodimeric subunits arrange them into a single column, the protofilament, and the protofilaments form lateral contacts to close into the required tubular structure. Inside a cell, usually 13 protofilaments combine to form a MT although deviations from this number are possible. *In vitro*, the MTs can have a variable number of protofilaments but the average number, in this case also, is around 13. Experiments reveal that the arrangement of heterodimers in adjacent protofilaments is slightly staggered, thus causing the MT to be arranged in a helical lattice. The protofilaments fit together laterally such that the neighbouring subunits follow three-start (or five-start) helices, i.e. during each complete turn of the helix the pitch of the helix rises by three (or five) subunits.

An interesting consequence of the heterodimeric structure of the MT is that it

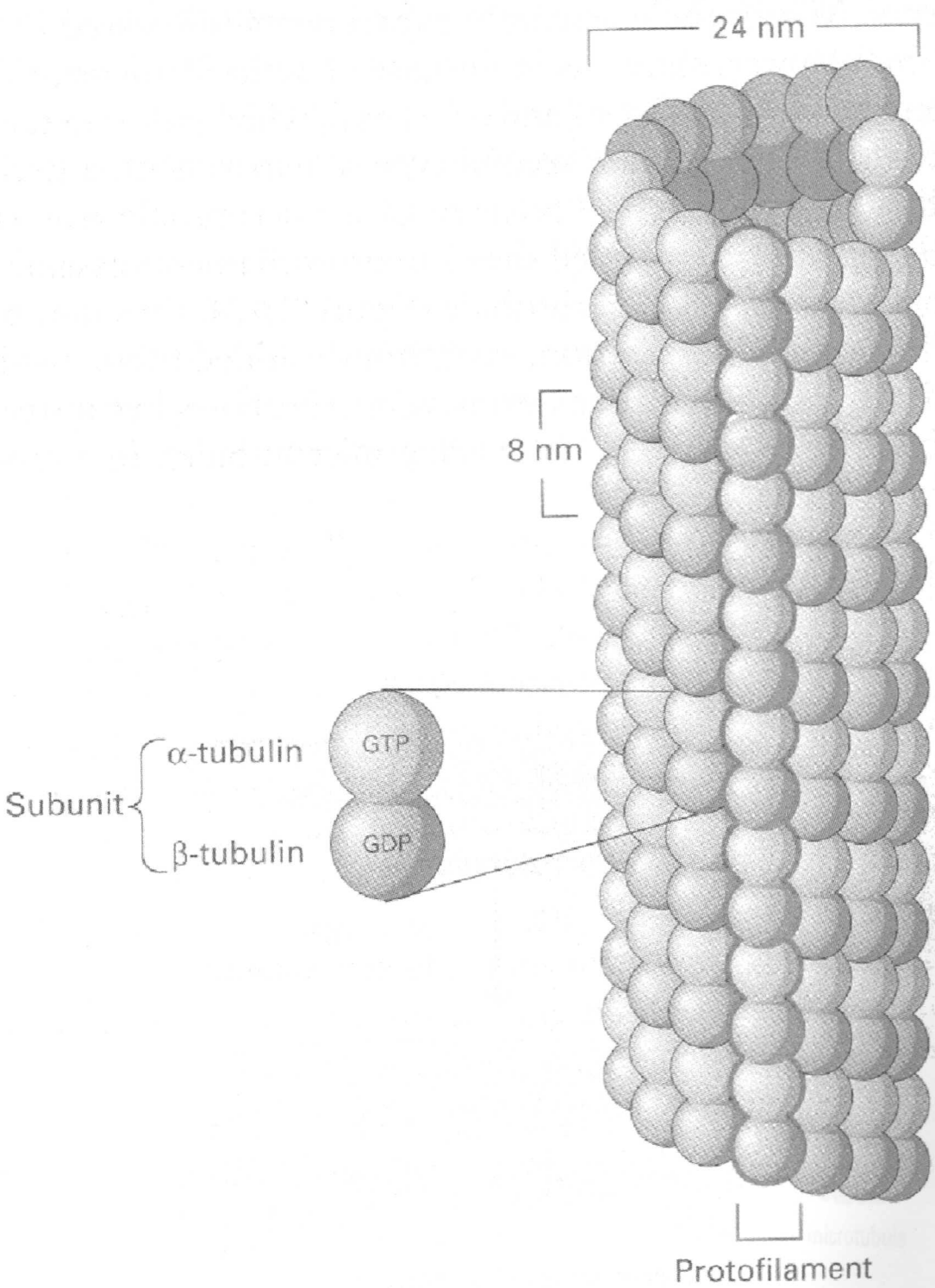

Figure 1.2: The organisation of subunits in a microtubule (Reproduced from Lodish et.al. Chapter 23)

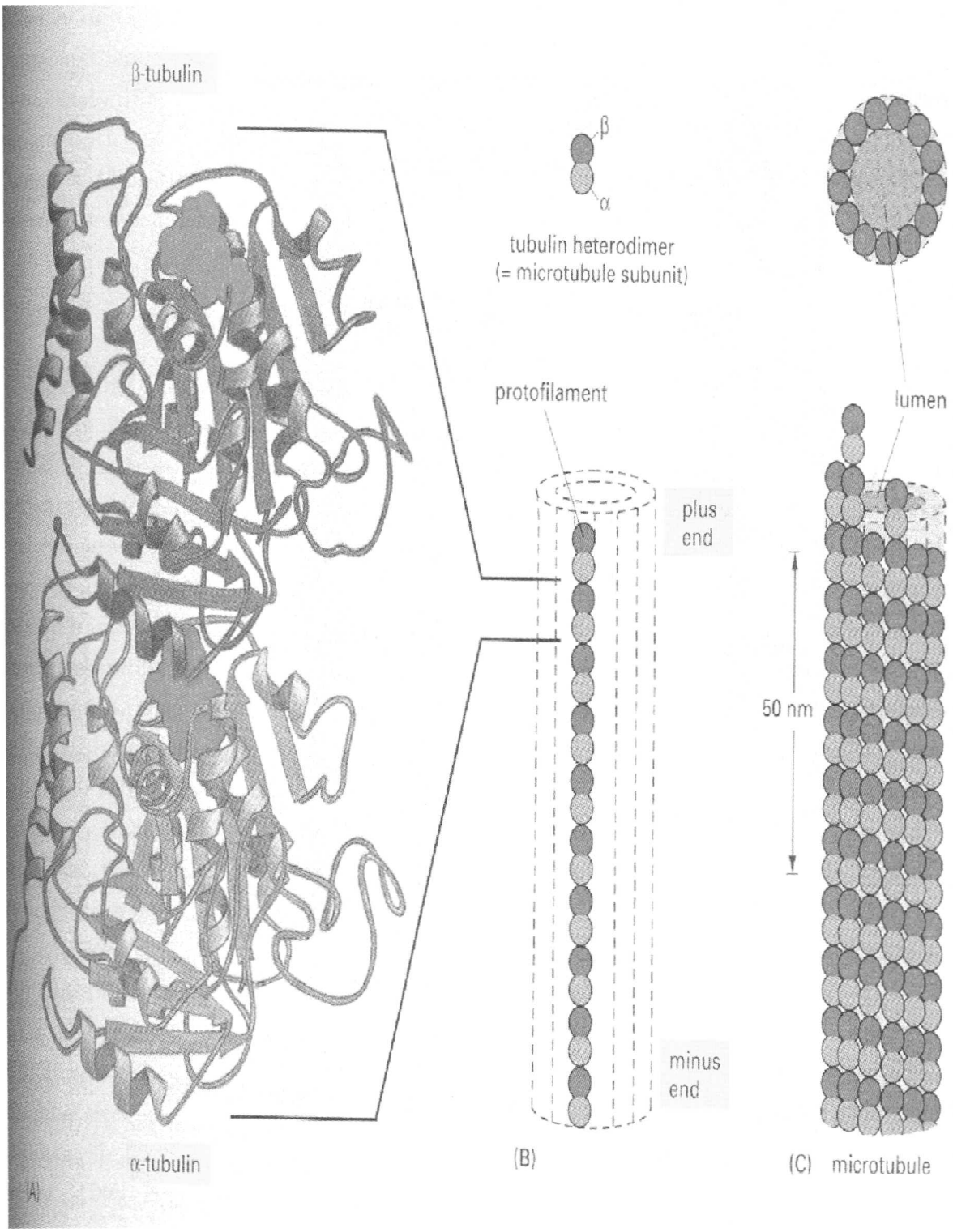

Figure 1.3: Structure of tubulin dimers and their arrangement into a MT (Reproduced from Alberts et. al. Chapter 16)

lends to the microtubule a certain structural polarity, depending on which monomer, the α or the β is exposed at the end of the tube. The end with the α-monomer exposed is known as the '-'end, and the β-tubulin end is known as the '+'end, the two ends differing in their rates of assembly. *In vitro,* MTs self-nucleate and grow from both ends, with the plus end growing more quickly. *In vivo,* the MTs nucleate from a Microtubule Organising Centre (MTOC) present in the cell such that the minus end remains anchored to the MTOC.

1.3 Dynamic Instability of Microtubules

The ability of the microtubules to grow and shrink very rapidly is critical for the efficient performance of the diverse functions of the MT. Thus a MT can have large scale length fluctuations which are comparable to the size of the MT itself. The microtubule can, under appropriate conditions constantly switch between assembly and disassembly states. This phenomenon of out-of-equilibrium aggregation is termed as "dynamic instability" (Mitchison and Kirschner, 1984). In all cases, microtubule growth is slow, and shrinking is rapid. Thus, a plot of the length of a microtubule with time resembles a sawtooth, and this apparently random phenomenon occurs both *in vivo* and *in vitro.* In a small region of the cell, at the same tubulin concentration, some microtubules will be growing longer, while others will be shrinking in length. Also, a single MT, over a period of time will go from the growing to the shrinking phases and vice versa. The transition from growth to shrinkage is termed as "catastrophe", whereas the reverse process of transition from shrinkage to growth is termed "rescue" (Dogterom and Leibler, 1993).

In vitro and *in vivo,* MTs polymerize by the addition of tubulin heterodimers. At the point of addition, the tubulin dimer is liganded with two molecules of GTP, but after incorporation into the MT lattice, the dimer is liganded by one molecule of GTP and one molecule of GDP, due to the hydrolysis of the GTP molecule liganded to the exchangeable site (E-site) at the β-monomer. It is now believed that this hydrolysis causes a straight-to curved configurational change in the dimer (Caplow et al., 1994; Hyman et al., 1995). However, due to the constraints of the MT lattice,

this curved configuration cannot be achieved, and the excess energy is stored in the MT's wall (Fygenson, 2001), thus poising the MT towards depolymerization (Jánosi et al., 2002). The process of rescue is not particularly well understood, but is believed to take place in a random manner.

1.4 The physics of Microtubule dynamics

There is as yet no comprehensive understanding of the phenomenon of dynamic instability of microtubules, or of the reasons why it makes transitions from the growth to the shrinkage states or vice versa. The dynamic instability process is evidently a non-equilibrium phenomena and as such can be studied using the methods of non-equilibrium statistical mechanics. Physical models of microtubule structure may help to elucidate the energetics of the MT lattice, and explain open problems such as how a microtubule is stabilised, or provide an explanation for the process of rescue.

Chapter 2

CAP MODELS FOR MICROTUBULES

2.1 Necessity for a stabilising cap

The processes of growth and shrinkage of microtubules do not occur by the same method. Growing microtubules display sheets of various lengths, widths, and curvatures at their extremities. On the other hand, depolymerization experiments reveal that microtubules depolymerize by release of short protofilament segments in a highly curved conformation. The present understanding of these phenomena is as follows: MTs polymerize from tubulin dimers liganded with two units of GTP, but after assimilation into the MT lattice, the dimers contain one unit of GTP and one unit of GDP, due to the hydrolysis of the GTP molecule on the E-site of the β-tubulin to GDP. This hydrolysis is believed to cause a straight-to-curved configurational change of the dimer. Thus the bulk of the MT lattice has a hidden intrinsic curvature, a hypothesis which is supported by the curved configuration of the oligomers released from the depolymerizing microtubule ends. This intrinsic curvature is unable to manifest itself in the MT because the protofilaments are bound laterally to each other in the MT wall, and the sheet of protofilaments curves laterally strongly to form the MT. Thus a microtubule has opposing intrinsic curvatures, the lateral curvature that favours

the formation of the tube, and the longitudinal curvature that prefers the protofilaments to be curved outside the tube. The resultant tube is the result of these two opposing curvatures, and mathematically, the sheet is said to have a negative Gaussian curvature. The hidden intrinsic longitudinal curvature poises the MT towards depolymerization and thus there must be some sort of "*cap*" at the end of the MT lattice which binds together the tube and allows polymerization to take place. The exact nature of this stabilising cap is not known for sure and has generated a lot of debate since the early days of dynamic instability. There are a lot of candidates for the stabilising cap and in this chapter we will be reviewing the main proposals.

2.2 The GTP cap Model

The GTP cap model was proposed originally by Mitchison and Kirschner (1984). This model proposes that transitions between the growth and shrinkage state occur due to competition between assembly and GTP hydrolysis. A growing MT assembles by the addition of tubulin subunits containing GTP molecules, which is then hydrolysed to GDP. According to the GTP cap model, a growing MT has a cap of GTP at its ends which is due to the time taken for the GTP molecules to hydrolyse to GDP. If hydrolysis overtakes the addition of new GTP tubulin, the cap is gone and the microtubule passes to the depolymerizing state, which is known as the catastrophe (Figures 2.1, 2.2). Thus according to this hypothesis, the hydrolysis of GTP to GDP is the rate limiting process that pushes the MT towards depolymerization. Although it is clear that GTP-hydrolysis precedes disassembly, it is not clear whether it is this process which is the rate determining step (Flyvbjerg et al., 1996).

Also there is a debate on the size of the GTP cap that is required to stabilise the microtubule. Experimentally, it is found that when MTs are grown in pure GTP-tubulin solutions at various constant concentrations, the frequency of catastrophes is one every few minutes and decreases with increasing concentration. This suggests that the stabilising cap is longer and hence less apt to be lost at larger concentrations. On the other hand, in dilution experiments, the concentration of tubulin is abruptly reduced to zero, resulting on catastrophes within seconds, independent of

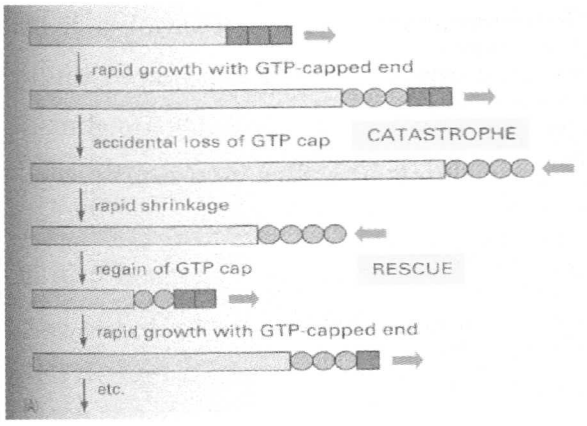

Figure 2.1: Schematic representation of the GTP cap hypothesis (Reproduced from Alberts et. al. Chapter 16)

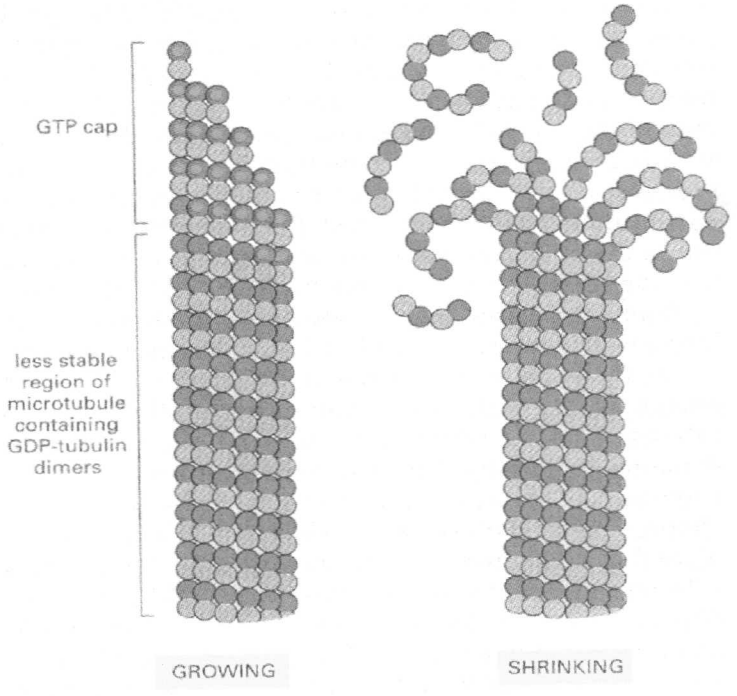

Figure 2.2: The GTP cap in a MT and depolymerization in its absence (Reproduced from Alberts et. al. Chapter 16)

the initial concentration. This suggests that the cap is short and independent of the concentration at which it is formed. Thus, it is not clear whether, if the GTP cap model is correct, it would require a long cap or whether a small cap would suffice. Recent results seem to indicate that if the stabilising cap is indeed a GTP cap, then a small (even single-layer) cap would suffice to stabilise the MT lattice (Caplow and Shanks, 1996).

Recently there has also been a debate as to the actual chemical composition of the cap at the end of the MT. Certain experiments seemed to suggest that instead of GTP, it is actually a GDP-P(i) (GDP + inorganic phosphate) complex that serves as the cap. Thus, according to this point of view, microtubules are capped with a tubulin-GDP-P(i) subunit at the end of its 13 protofilaments and this is responsible for stabilising microtubules in the growth phase. It was concluded that P(i) in terminal tubulin-GDP-P(i) subunits does not exchange with the solvent (Panda et al., 2002). However, contrary results from other experiments put a doubt on the ability of tubulin-GDP-P(i) subunits to stabilise microtubules (Caplow and Fee, 2003).

2.3 The Structural cap Model

The structural cap model proposes that there is scope for stabilising the microtubule lattice if the structure at the ends of the MT is slightly different from that along the length of the tube. This is possible because there is a scope for stress-release at the ends due to bending of the protofilaments as an expression of the hidden intrinsic curvature of MT walls. Experiments on growing microtubules show that the ends of growing MTs are heterogeneous during assembly, ranging from blunt ends to long curved extensions up to several micrometers in length. Microtubule assembly therefore seems to occur by addition of tubulin subunits to curved sheets that close into a tube (Chrétien et al., 1995).

Studies of microtubule dynamics have shown that catastrophes are suppressed by increasing growth rate (Mitchison and Kirschner, 1984). On the other hand, structural studies reveal that the length of the sheets at the ends of the MT increases with increasing growth rate (Chrétien et al., 1995). These two facts taken together

seem to indicate that longer sheets at the end of growing microtubules correlate with increased stability of the MT (Figure 2.3). Furthermore, the lengths of the sheets at any particular tubulin concentration are variable from microtubule to microtubule, suggesting a stochastic rate of tube closure. Thus, if the sheet were, on an average, shorter, there would be more chance that during a stochastic period of closure, the tube closes all the way to the end. If closure of the tube to the end of the MT simulated catastrophe, a stochastic rate of tube closure would then determine a stochastic rate of catastrophes. This model is known as the Structural cap model because it predicts that the dynamic properties of microtubules are regulated by the structure at the microtubule ends and not simply by the rate constants of addition of GTP tubulin and GDP tubulin (Hyman and Karsenti, 1996). A possible explanation of why tube closure triggers microtubule depolymerization is that the sheet has an inherently stable configuration, while the tube is inherently unstable. Thus when tube closure occurs, if sufficient GTP is hydrolysed, then this can trigger depolymerization.

However, as proposed by Jánosi *et. al.* (Jánosi et al., 2002), stress release does not require a complicated end structure such as sheet like extensions at the end of the MT. Blunt MT ends can also lower their elastic energy by adopting a relaxed configuration, plus- and minus-ends alike. This local relaxation amounts to a structural cap, and is independent of the chemical composition of the MT ends. The MT is modelled as a two-dimensional elastic sheet with opposite intrinsic curvatures (Jánosi et al., 1998). Janosi et. al. use a filament model to show that this elastic tube is capped by a structure different from its bulk: it displays a structural cap. They also propose the existence of a so-called "third state" or quiescent state, in which the microtubule neither grows nor shrinks. When GTP-liganded tubulin is lost from the ends, the MT is left in the meta-stable state that results due to the competition between the two opposing curvatures. This state leaves for the depolymerizing state only when a random thermal excitation pushes it over the barrier toward depolymerization. They also propose a possible mechanism for "rescue", the transition from the depolymerization state to the polymerizing state. They propose that the phenomenon of rescue occurs due to random thermal fluctuations. Since thermal fluctuations can remove energy from the system apart from adding energy to the system, and both these processes

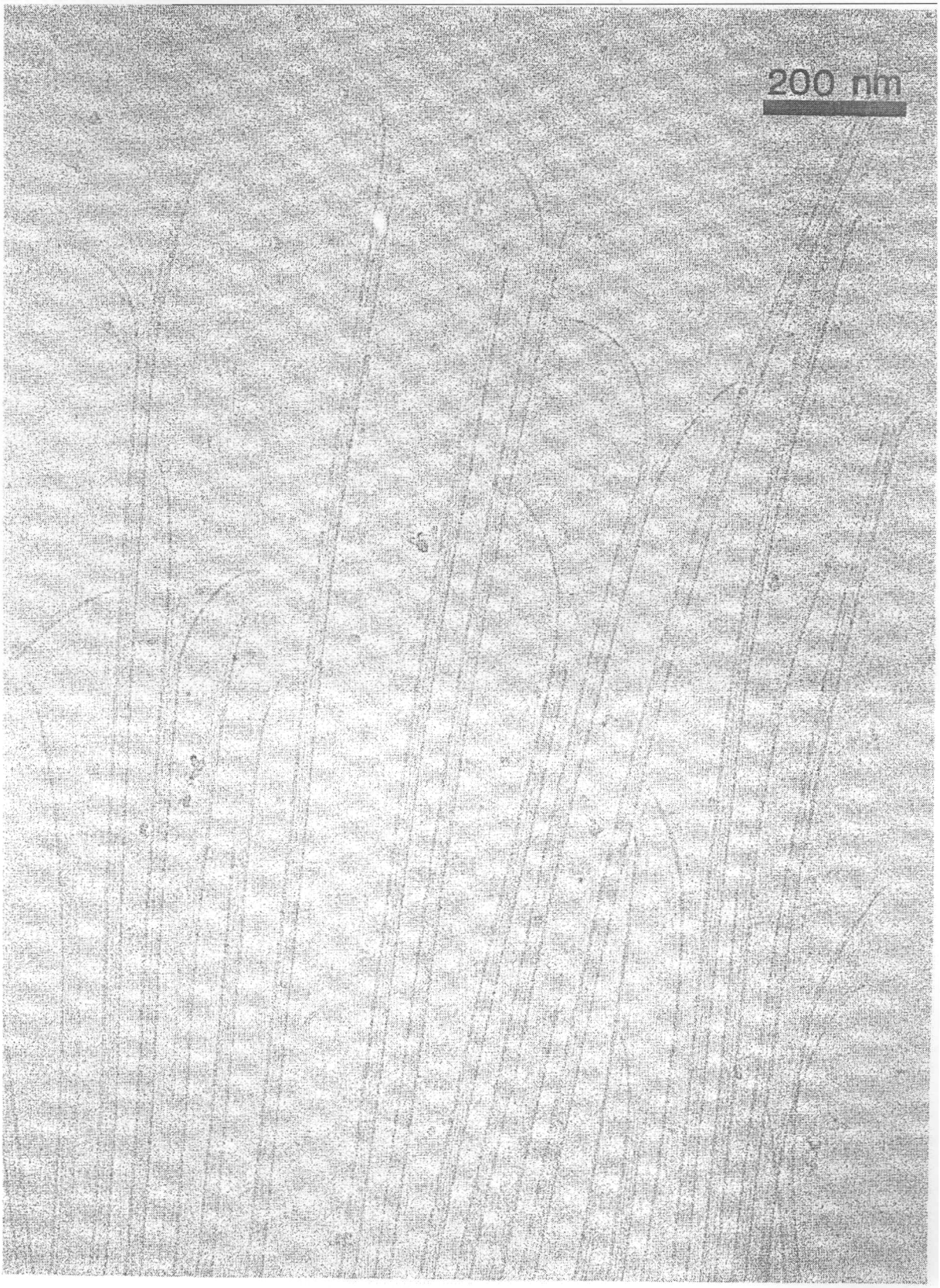

Figure 2.3: Experimental picture of MT end. The ends range from blunt to long, narrow tips, formed by sheets of microtubule wall. (Reproduced from Janosi et. al., 1998)

are random, thus the rescue mechanism can be random.

2.4 A Combination of Conformational and GTP caps

It is possible that the stabilising cap is a combination of both the structural and the GTP caps. According to this hypothesis, the structural cap contributes to the microtubule stability by allowing for a more relaxed structure near the ends of the MT. However, even with the structural cap, it is possible that the ends of the curved sheets contains a few layers of GTP molecules, which also contribute to the stability of the microtubule, thus forming the mixed GTP-conformational cap (Tran et al., 1997). However, if the GTP molecules do indeed occur at the ends of the curved sheets, it should be noted that their only direct effect is on the sheet, while the sheet contributes to the stability of the microtubule (Chrétien et al., 1999). In fact, within their filament model, Jánosi *et. al.* (2002) show that the GTP cap stabilises an MT simply by being intrinsically straight, and it does this quite efficiently, exponentially in the cap size.

Chapter 3

MATERIALS AND METHODS

We have carried out Monte-Carlo (MC) and Brownian Dynamics (BD) simulation of the MT lattice and studied the equilibrium structure both at zero temperature and at finite temperatures, with special emphasis on the structure at the ends of the microtubule. Such simulations should be able to determine whether stress release occurs at the ends of the microtubule by protofilament bending and hence provide a test for the Structural Cap Model.

3.1 The Model

Our model consists of tubulin subunits placed along a cylindrical lattice. The coordinates of the centre of each subunit is specified, and 13 units are placed on a single ring. The MT is then constructed by placing 'n' such rings on top of each other. Each unit is connected by springs to its four nearest neighbours, two on either side of the same ring, and the two at the top and bottom of the two adjacent rings. The springs in the horizontal direction differ from those in the vertical direction in their nature, spring constants, and equilibrium distances. The bonds have a preferred bond length and preferred bond angles both in the lateral and longitudinal directions. The preferred bond angles in the lateral direction ensures that the units close around to form a cylinder. The preferred bond angle in the vertical direction, if present, expresses the fact that the microtubule has an intrinsic curvature in the longitudinal direction

due to conformational changes on hydrolysis of the GTP molecules. This intrinsic curvature can also be set to zero in order to model MTs constituted of material with zero internal curvature. The springs along the lateral direction can be either linear or non-linear in nature, and the differences, if any between the two cases can be studied. In addition, we introduce an explicit term that enforces self-avoidance in the MT lattice. Also we add an energy term that penalises deviations from the square topology of the lattice and study the combined effects of these various terms on the equilibrium structure of the microtubule. For the time being, we neglect the helical character of the microtubule but this can be accommodated through a straightforward generalisation of the approach presented here.

The various interactions between the tubulin subunits of the microtubule are modelled in the following way:

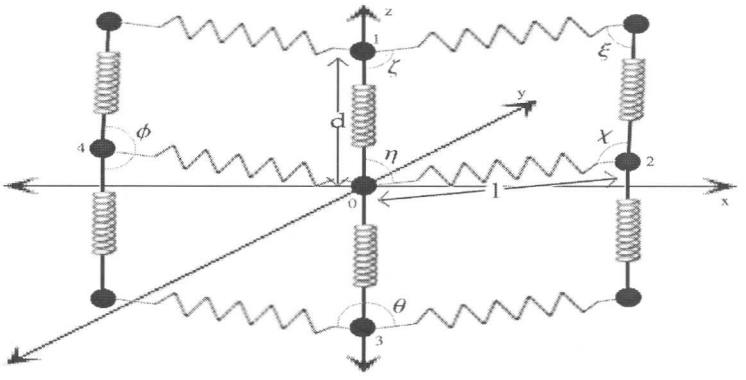

Figure 3.1: A schematic figure showing the different springs connecting the atoms in the MT lattice and the various lengths and angles

- Within any one given ring, the angle between two adjacent bonds (a three-body interaction) has a preferred value, with the energy cost being quadratic in the difference of the cosines. Then, if the bond angle is "θ" and the equilibrium value is "θ_0", the energy can be written as,

$$E_{lat,bending} = \frac{1}{2} K_{lat,b} (cos\theta - cos\theta_0)^2$$

- Within any one given ring, the bond length between two atoms has a preferred value, and the energy cost can be either linear or non-linear in the deviation.

  - Linear spring:
    If the bond length is "l" and the equilibrium length is "l_0", the energy can be written as,
    $$E_{lat,stretching} = \frac{1}{2} K_{lat,s}(l - l_0)^2$$
  - Nonlinear spring:
    If the bond length is "l" and the equilibrium length is "l_0", the energy can be written as,
    $$\begin{aligned} E_{lat,stretching} = & [\frac{1}{2} K^1_{lat,s}(l - l_0)^2] \\ & -[\frac{1}{2} K^2_{lat,s}(l - l_0)^3] \\ & +[\frac{1}{2} K^3_{lat,s}(l - l_0)^4] \end{aligned}$$
    This form of the energy implies that a displacement which increases the bond length from its equilibrium value is penalised less than one which decreases the bond length.

- Between any three adjacent rings, the bond angles between two adjacent bonds has an optimum value, and the energy cost is quadratic in the difference between the cosines. Then, if the bond angle is ϕ, and the equilibrium value is ϕ_0, the energy can be expressed as
  $$E_{long,bending} = \frac{1}{2} K_{long,b}(cos\phi - cos\phi_0)^2$$

- The bond length between two corresponding subunits in two adjacent rings has an equilibrium value d_0 (say), and the energy cost is quadratic in the difference. Then, if the actual bond length is d, the energy is,
  $$E_{long,stretching} = \frac{1}{2} K_{long,s}(d - d_0)^2$$

- With the inclusion of an explicit self-avoidance term in the model, the stretching energy costs are modified and can be expressed as,

$$E^{self-avoiding}_{lat,stretching} = E_{lat,stretching} + \frac{K_{SA}}{r^{12}}$$
$$E^{self-avoiding}_{long,stretching} = E_{long,stretching} + \frac{K_{SA}}{r^{12}}$$

- The square lattice connected by springs has an inherent instability (Plischke et al., 1999) in the ground state in that it has infinitely degenerate ground state configurations which can be accessed by gradually deforming the square into a parallelogram and squishing it correspondingly. In order to break this degeneracy, we add an energy term in our model that penalises deviations from the square topology of the lattice bonds. Thus if we consider any particle in the lattice, it has 4 bonds with its four nearest neighbours. If we denote the angles that these bonds mutually make amongst themselves as η, ζ, ξ, and χ respectively, then the energy cost of deviations from the perfect square topology can be expressed as

$$\begin{aligned} E_{topology} = \frac{1}{2}K_{topo.} \quad \times \quad & [(cos\eta - cos\frac{\pi}{2})^2 + (cos\zeta - cos\frac{\pi}{2})^2 \\ + \quad & (cos\xi - cos\frac{\pi}{2})^2 + (cos\chi - cos\frac{\pi}{2})^2] \end{aligned}$$

The final structure of the microtubule lattice is then determined by the competition between the above listed energy terms.

3.2 The principle of Monte-Carlo simulations

The properties of many molecular systems can be described by a separable Hamiltonian of the general form

$$H(q,p) = E_k(p) + E_p(q)$$

where E_k and E_p are the kinetic and potential energies and q and p denote the position and momentum vectors of the system. This hamiltonian function forms the basis for MC simulations applied to estimate various properties of large molecular systems.

The MC estimates must emulate a probability density function $\rho(q,t)$ or $\rho(q,p,t)$ appropriate for a statistical ensemble. MC simulations must generate an ensemble around a statistical equilibrium. The equilibrium ensemble regime is appropriate when $\rho(X,t) = \rho_0(X)$ for some $t > t_0$, where X represents the collective phase space vector of the system. The ensemble average is then considered as an estimate for the time average (which may be much more difficult to follow), a statement of the *Ergodic hypothesis*. In this statistical equilibrium case, the rule that generates X_{n+1} from X_n need not have a clear physical interpretation. However, to be useful for sampling, the rule must ensure that the starting distribution $\rho(X,t)$ should tend to the stationary density $\rho_0(X)$ and that the system be ergodic (i.e. over time, the system should visit all phase space cells with equal probability).

The probability density function for the canonical ensemble is proportional to the Boltzmann factor,

$$\rho(X) \propto exp(-\beta E(X))$$

where E is the total energy of the system and $\beta = (1/k_B T)$.
Hence for two system states X and X', the corresponding probability ratio is

$$\frac{\rho(X)}{\rho(X')} = exp(-\beta \Delta E),$$

where

$$\Delta E = E(X) - E(X').$$

The corresponding means for the system for a function A can then be written as

$$\langle A(x) \rangle = \int \rho(x) A(x) dx.$$

The Metropolis algorithm described below is used to generate an appropriate Markov chain from which the expectation value of A is calculated as

$$\langle A(x) \rangle = \lim_{M \to \infty} \frac{1}{M} \sum_{i=1}^{M} (A(x_i))$$

Metropolis described an efficient and elegantly simple procedure for the canonical ensemble. In mathematical terms, we generate a Markov chain of molecular

states $X_1, X_2, X_3, ...$ constructed to have the limiting distribution $\rho(X)$. In a Markov chain, the outcome X_{n+1} depends only on X_n. The Metropolis algorithm constructs a transition matrix for the Markov chain that is stochastic and ergodic so that the limiting distribution for each state X_i is $\rho_i = \rho(X_i)$ and thereby generate a phase space trajectory in the canonical ensemble.

The Metropolis algorithm generates a trial $\tilde{X}_{i+1}$ from X_i by a system-appropriate random perturbation and accepts the state if the corresponding energy is lower. If however, $E(\tilde{X}_{i+1}) > E(X_i)$, then the new state is accepted with probability p = $\exp(-\beta\Delta E)$, where $\Delta E = E(\tilde{X}_{i+1}) - E(X_i) > 0$, by comparing p to a uniformly generated number on the (0:1) interval. In this manner, states with lower energies are always accepted but some states with higher energies have a nonzero probability of acceptance too. Consequently, the sequence tends to regions of configuration space with low energies, but the system can always escape to other energy basins.

3.3 The principle of Brownian dynamics

3.3.1 The Langevin Equation of motion

The basic equation behind the Brownian Dynamics simulation is the Langevin Equation of motion. The Langevin equation is a stochastic differential equation in which two force terms have been added to Newton's second law of motion to approximate the effects of the neglected degrees of freedom. The effects of the solvent molecules not explicitly present on the system being simulated would be approximated in terms of a frictional drag on the solute as well as random kicks associated with the thermal motions of the solvent molecules. Thus the Langevin equation of motion is Newton's second law with three forces acting on the particles: viscous damping, random thermal noise, and a systematic force. Then, Langevin's equation for the motion of particle i is:

$$\vec{F}_i^s(t) - \Gamma_i \vec{v_i}(t) + \vec{F}_i^r(t) = m_i \dot{\vec{v}}_i(t)$$

where,

$\vec{F}_i^s(t)$ is the systematic force on the i^{th} particle at time t, i.e., the force on the i^{th}

particle due to all other particles explicitly present in the system;
$\vec{F_i^r}(t)$ is the random force on the i^{th} particle at time t used to induce thermal fluctuations in the energy of the particle;
$\vec{v_i}(t)$ is the velocity of the i^{th} particle at time t;
Γ_i is the coefficient of friction for the i^{th} particle.

In one-dimension, the Langevin equation reads:

$$F_i^s(t) - \Gamma_i v_i(t) + F_i^r(t) = m_i \dot{v}_i(t)$$

This equation can be factored as

$$me^{-\Gamma t/m}\frac{d}{dt}[e^{\Gamma t/m}v] = F^r + F^s$$

and has the general solution:

$$v(t) = e^{-\Gamma t/m}\left[v(0) + \frac{1}{m}\int_0^t e^{\Gamma s/m}(F^r(s) + F^s(s))ds\right]$$

If we assume that the random force is a white noise process, then its correlation can be described by:

$$\langle F^r(s_1)F^r(s_2)\rangle = A\delta(s_1 - s_2)$$

Then, the correlation in particle velocities can be expressed as:

$$\langle v(t_1)v(t_2)\rangle = v^2(0)e^{-\Gamma(t_1+t_2)/m} + \frac{A}{2\Gamma m}\left[e^{-\Gamma|t_1-t_2|/m} - e^{-\Gamma(t_1+t_2)/m}\right]$$

To obtain the mean kinetic energy, we take $t_1 = t_2 =$ t. This gives,

$$\langle v^2(t)\rangle = v^2(0)e^{-2\Gamma t/m} + \frac{A}{2m\Gamma}[1 - e^{-2\Gamma t/m}]$$

At equilibrium, i.e. in the limit t $\to \infty$ this value approaches

$$\langle v^2(t)\rangle = \frac{A}{2m\Gamma}$$

Now, from the equipartition theorem, we know $\langle v^2\rangle = \frac{k_B T}{m}$.
Thus, we obtain, $A = 2\Gamma k_B T$.
Then, the random force is described by the variance

$$\langle F^r(s_1)F^r(s_2)\rangle = 2\Gamma k_B T\delta(s_1 - s_2)$$

which is a statement of the fluctuation-dissipation theorem. At thermal equilibrium, the strength of the random thermal noise must be proportional to the frictional damping constant. Alternately, if the friction coefficient is known, the width of the distribution sets a temperature scale in the problem.

3.3.2 The Algorithm for the simulation

For the Brownian Dynamics simulation, we work in the overdamped limit, i.e. we assume that the acceleration of each particle is zero. Then, putting $\dot{\vec{v}} = 0$, in the Langevin equation, we get,

$$\vec{v}(t) = \frac{1}{\Gamma}(\vec{F}^s(t) + \vec{F}^r(t))$$

Now, we start with an initial configuration of the particles (n $\times$ 13). Then, we calculate the systematic force (F^s) on each particle due to all the other particles. We then generate a random force (F^r) from a Gaussian distribution and calculate the velocity on each particle in accordance with the formula given above. Then we update the position of each particle according as,

$$R_a(t + \Delta t) = R_a(t) + V_a \Delta t, \qquad a \in \{x, y, z\}$$

where the time-step Δt is chosen such that a typical displacement in one time-step is a small fraction of the interparticle spacing. The system is then allowed to evolve over a period of time until a equilibrium structure is generated and then the properties of the equilibrium structure was studied.

3.4 Finite temperature simulations: Setting the temperature scale

When performing the finite temperature simulations, it is important to know what the typical temperature scale of the system is. If the temperature of the system is too high, thermal fluctuations will be too high and this can destroy the order of the microtubule. Again, for too low temperatures, the system can take very long time to equilibrate and can thus take an inordinate amount of computing time.

To calculate the typical temperature scale of the system, we consider any one particle, and the four neighbouring particles it is bonded to (refer to figure 3.1). We calculate the effective potential at the central particle due to its neighbouring particles. The effective spring constants for small displacements of the central particle about its equilibrium position is obtained from the value of the second derivative of the effective potential about the equilibrium position.

$$
\begin{aligned}
E_{01} &= \frac{1}{2}K_{lat,s}[\sqrt{(x-x_1)^2+(y-y_1)^2+(z-z_1)^2}-a]^2 \\
E_{03} &= \frac{1}{2}K_{lat,s}[\sqrt{(x-x_3)^2+(y-y_3)^2+(z-z_3)^2}-a]^2 \\
E_{02} &= \frac{1}{2}K^1_{long,s}[\sqrt{(x-x_2)^2+(y-y_2)^2+(z-z_2)^2}-b]^2 \\
&\quad -\frac{1}{2}K^2_{long,s}[\sqrt{(x-x_2)^2+(y-y_2)^2+(z-z_2)^2}-b]^3 \\
&\quad +\frac{1}{2}K^3_{long,s}[\sqrt{(x-x_2)^2+(y-y_2)^2+(z-z_2)^2}-b]^4 \\
E_{04} &= \frac{1}{2}K^1_{long,s}[\sqrt{(x-x_4)^2+(y-y_4)^2+(z-z_4)^2}-b]^2 \\
&\quad -\frac{1}{2}K^2_{long,s}[\sqrt{(x-x_4)^2+(y-y_4)^2+(z-z_4)^2}-b]^3 \\
&\quad +\frac{1}{2}K^3_{long,s}[\sqrt{(x-x_4)^2+(y-y_4)^2+(z-z_2)^4}-b]^4
\end{aligned}
$$

The total energy is then,

$$E[x,y,z] = E_{01} + E_{02} + E_{03} + E_{04}$$

Assume, $K_{lat,s} = K^1_{long,s} = K^2_{long,s} = K^3_{long,s} = 1$.

Then,

$$\begin{aligned}
\frac{\partial E_{01}}{\partial x} &= \left[\sqrt{(x-x_1)^2+(y-y_1)^2+(z-z_1)^2}-a\right] \\
&\times \frac{(x-x_1)}{\sqrt{(x-x_1)^2+(y-y_1)^2+(z-z_1)^2}} \\
\frac{\partial^2 E_{01}}{\partial^2 x} &= \left[\frac{(x-x_1)}{\sqrt{(x-x_1)^2+(y-y_1)^2+(z-z_1)^2}}\right]^2 \\
&+ \left[\frac{\sqrt{(x-x_1)^2+(y-y_1)^2+(z-z_1)^2}-a}{\sqrt{(x-x_1)^2+(y-y_1)^2+(z-z_1)^2}}\right] \\
&- \left[\frac{[\sqrt{(x-x_1)^2+(y-y_1)^2+(z-z_1)^2}-a](x-x_1)^2}{[(x-x_1)^2+(y-y_1)^2+(z-z_1)^2]^{3/2}}\right] \\
\frac{\partial^2 E_{01}}{\partial^2 x}|_0 &= \frac{x_1^2}{\sqrt{(x-x_1)^2+(y-y_1)^2+(z-z_1)^2}} \\
&+ \frac{\sqrt{(x-x_1)^2+(y-y_1)^2+(z-z_1)^2}-a}{\sqrt{(x-x_1)^2+(y-y_1)^2+(z-z_1)^2}} \\
&- \frac{x_1^2[\sqrt{(x-x_1)^2+(y-y_1)^2+(z-z_1)^2}-a]}{[(x-x_1)^2+(y-y_1)^2+(z-z_1)^2]^{3/2}} \\
\Rightarrow \frac{\partial^2 E_{01}}{\partial^2 x}|_0 &= \frac{x_1^2}{a}
\end{aligned}$$

Similarly,

$$\frac{\partial^2 E_{03}}{\partial^2 x}|_0 = \frac{x_3^2}{a}, \quad \frac{\partial^2 E_{01}}{\partial^2 y}|_0 = \frac{y_1^2}{a}, \quad \frac{\partial^2 E_{03}}{\partial^2 y}|_0 = \frac{y_1^2}{a}, \quad \ldots$$

Again,

$$\begin{aligned}
\frac{\partial E_{02}}{\partial x} &= \{[\sqrt{(x-x_2)^2+(y-y_2)^2+(z-z_2)^2}] \\
&- \frac{3}{2}[\sqrt{(x-x_2)^2+(y-y_2)^2+(z-z_2)^2}]^2 \\
&+ 2[\sqrt{(x-x_2)^2+(y-y_2)^2+(z-z_2)^2}]^3\} \\
&\times \frac{(x-x_2)}{\sqrt{(x-x_2)^2+(y-y_2)^2+(z-z_2)^2}}
\end{aligned}$$

On differentiating again and finally expanding about the equilibrium position, we have,

$$\frac{\partial^2 E_{02}}{\partial^2 x}|_0 = \frac{x_2^2}{b^2}$$

Similarly, we obtain

$$\frac{\partial^2 E_{02}}{\partial^2 y}|_0 = \frac{y_2^2}{b^2}, \quad \frac{\partial^2 E_{04}}{\partial^2 x}|_0 = \frac{x_4^2}{b^2}, \quad \frac{\partial^2 E_{04}}{\partial^2 y}|_0 = \frac{y_4^2}{b^2}, \quad \ldots$$

Thus, finally, we have,

$$\begin{aligned}
\frac{\partial^2 E}{\partial^2 x}|_0 &= \left(\frac{x_1^2 + x_3^2}{a^2}\right) + \left(\frac{x_2^2 + x_4^2}{b^2}\right) \\
&= \kappa_1 \ \text{(say)} \\
\frac{\partial^2 E}{\partial^2 y}|_0 &= \left(\frac{y_1^2 + y_3^2}{a^2}\right) + \left(\frac{y_2^2 + y_4^2}{b^2}\right) \\
&= \kappa_2 \ \text{(say)} \\
\frac{\partial^2 E}{\partial^2 z}|_0 &= \left(\frac{z_1^2 + z_3^2}{a^2}\right) + \left(\frac{z_2^2 + z_4^2}{b^2}\right) \\
&= \kappa_3 \ \text{(say)}
\end{aligned}$$

The effective spring constants κ_1, κ_2 and κ_3 are a measure of the response of the system to small deviations from the equilibrium position. Thus for deviations Δx, Δy, Δz from the equilibrium position, the energy cost is

$$E = \frac{1}{2}(\kappa_1 \Delta x^2 + \kappa_2 \Delta y^2 + \kappa_3 \Delta z^2)$$

This energy introduces a temperature scale in the system according as $E \sim k_B T_{ch}$ and this characteristic temperature provides an estimate of the temperature at which finite temperature simulations are to be performed.

Chapter 4

ELASTIC RESPONSE OF THE TUBE

In this chapter, we will subject the microtubule lattice to small deformations about its equilibrium position and study the elastic response of the tube to such small deformations. We shall calculate the free energy of the tube within our model as a function of the displacements and hence determine the elastic moduli of the tube.

To calculate the elastic response, we will choose the following version of our model. We will consider the tube to have a zero intrinsic curvature in the longitudinal direction, i.e. we assume that successive bonds along the longitudinal direction prefer to align themselves along a straight line. Also, we assume that the adjacent subunits on any given horizontal ring are attached to each other using linear springs. We consider the zero temperature equilibrium structure (Figure 5.4) and then measure the response to small deviations about this structure.

4.1 The Torsion Modulus

Firstly, we consider a "torsional deformation" of the structure. A torsional deformation is one in which, although the rod remains straight, each transverse section (i.e. in our model, each ring) is rotated through some angle relative to those below it (Landau and Lifshitz, 1986). If the cylinder is long, even a slight torsion causes

sufficiently distant cross-sections to turn through large angles. The generator of the sides of the cylinder, which are originally parallel to the axis, become helical in form under torsion.

Let us define the *torsion angle* τ, which is the angle of rotation per unit length of the tube. This means that two neighbouring rings at a distance dz will rotate through a relative angle $d\phi = \tau$ dz. The torsional deformation itself is assumed to be small. Within our model, this constraint is satisfied by ensuring that the maximum angular displacement, which occurs at the topmost ring of the tube, is a fraction of the equilibrium value of the inter-particle angle.

The torsional energy per unit length of the tube is given as $\frac{1}{2}C\tau^2$, where the constant C measures the response of the tube to the torsional deformation and is called the "torsional rigidity" of the tube. The total energy of the tube is then equal to the integral

$$F_{tube} = \frac{1}{2}\int C\tau^2 dz,$$

taken along the length of the tube.

Now, in the case under study, one end of the tube is held fixed and the external forces act only to the other end. These forces are such that they cause only a twisting of the tube, and no other deformation such as bending. We expect that, in such a case, the torsion angle τ is constant along the tube (Landau and Lifshitz, 1986). Then, if the length of the tube is L, the total angle of rotation of the upper end of the tube relative to the lower end is τL. The free energy is then,

$$F_{tube} = \frac{1}{2}C\tau^2 L$$

From this equation if all the other values are known, the torsional rigidity can be calculated.

To calculate this rigidity, firstly, we plot the values of the energy for different system sizes for a fixed value of the torsional angle ($\tau = 0.0001$). From the graph (Figure 4.1), it appears that the energy per unit length stabilises near the region n (number of rings in the tube) ≥ 400, and we choose to work with n=500 for further calculations. Then, with n = 500, we plot the Energy per unit length (E/L) against the value of the torsion angle τ (Figure 4.2). The value of the torsional rigidity is

obtained by plotting $\frac{2E}{L\tau^2}$ against τ (Figure 4.3) and reading off the value at which the plot stabilises.

Then, we plot the graph of $\frac{2E}{L\tau^2}$ against τ for different values of the various spring constants. Specifically, we vary the longitudinal stretching spring constant $K_{long.,s}$ (Figures 4.4), and the topology preserving spring constant K_{topo} (Figures 4.5). The curves for different values of the parameters $K_{lat.,b}, K_{lat.,s}$ and $K_{long.,b}$ are identical, because these springs remain at their equilibrium positions under the torsional displacement.

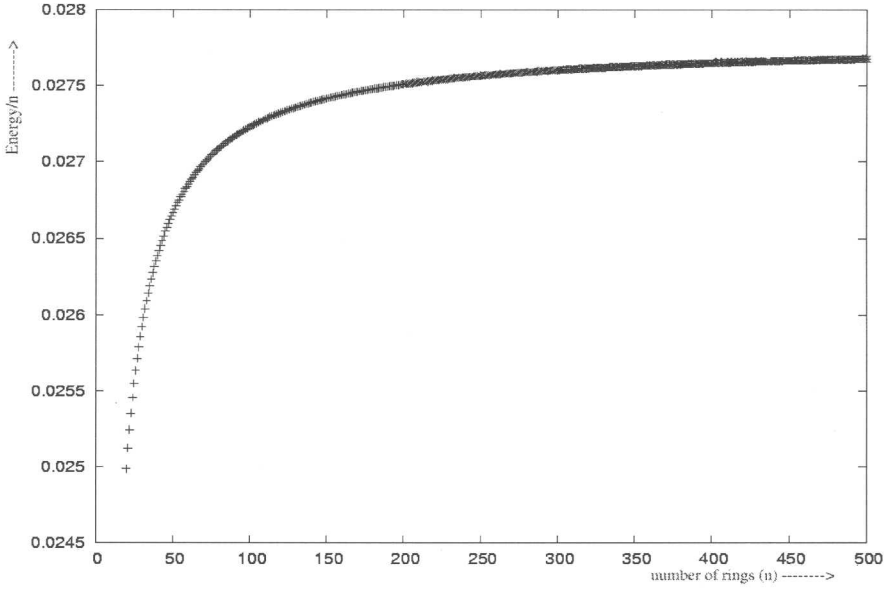

Figure 4.1: Energy values for different system sizes (torsion)

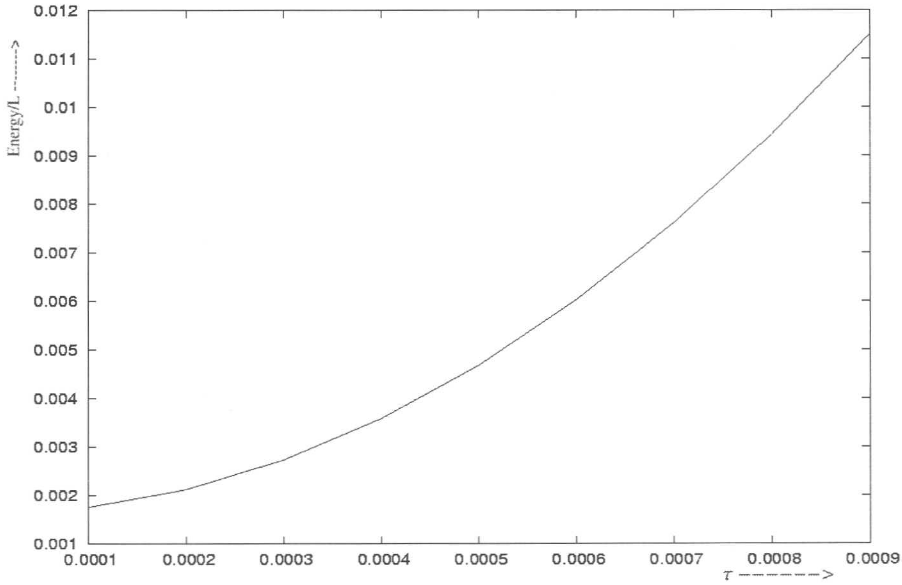

Figure 4.2: Energy/length for different torsion angles

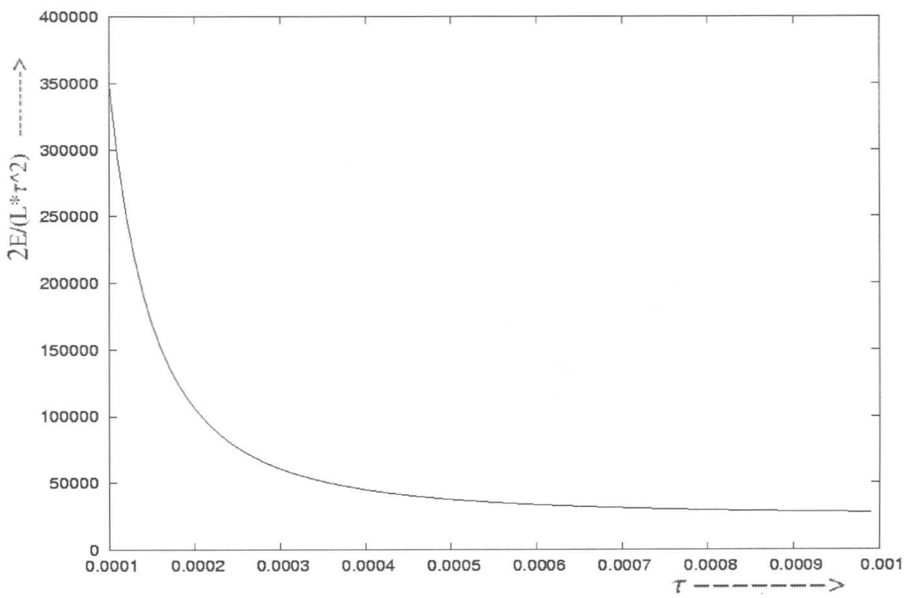

Figure 4.3: Energy/(L*τ^2) for different torsion angles

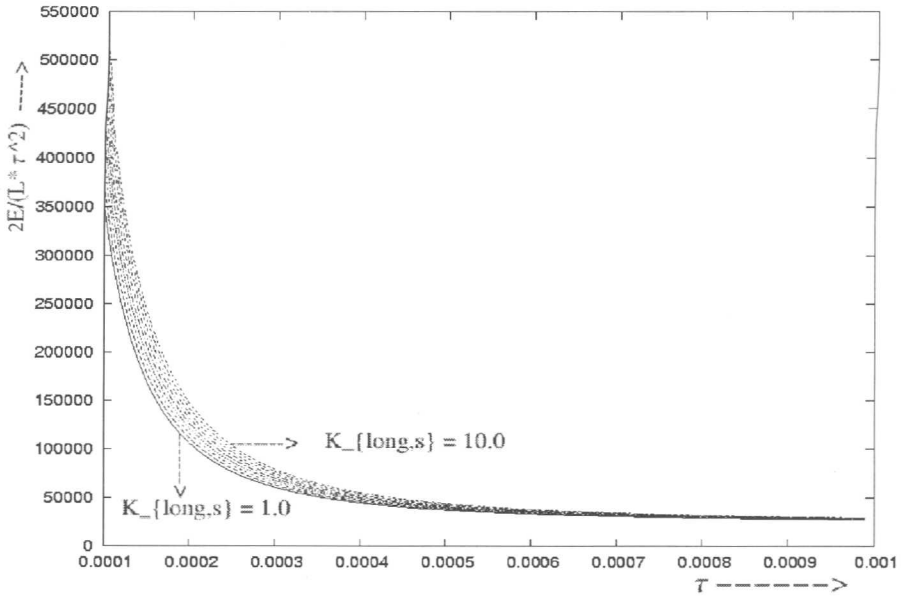

Figure 4.4: Energy/(L*τ^2) for different torsion angles at different $K_{long,s}$

Figure 4.5: Energy/(L*τ^2) for different torsion angles at different K_{topo}

4.2 The Tilt Modulus

Now consider a *tilt deformation* of the structure. A tilt deformation is defined as one, in which, each transverse section is shifted in a particular direction by some small amount relative to those below it. Thus the resultant structure is a tube whose axis is a straight line which is tilted at some constant angle with respect to the axis of the unperturbed cylinder.

We now define the *tilt variable* α which is a measure of the shift per unit length of the tube. Thus the centres of mass of two neighbouring rings are shifted by an amount dr = α dz. The variable α is chosen such that the amount the particles are shifted by in the topmost layer is a fraction of the radius of the tube.

The tilt energy per unit length of the tube is given by $\frac{1}{2}C_t\alpha^2$, where the constant C_t measures the response of the system to a tilt deformation and is called the "tilt modulus" of the system. The total energy of the system is then given by

$$E_{tube} = \frac{1}{2}\int C_t\alpha^2 dz$$

along the length of the tube. Moreover, as before, if the tilt variable α is a constant, then the total energy of the tube can be written as

$$E_{tube} = \frac{1}{2}C_t\alpha^2 L$$

where L is the total length of the tube.

To determine the tilt modulus, we follow the same procedure as before. Firstly, we plot the energy per unit ring against the number of rings (Figure 4.6) and from there determine the n at which to perform subsequent calculations (n=500). Then, given this n, we plot the energy per unit length against the tilt variable α (Figure 4.7) and also $\frac{2E}{L\alpha^2}$ against α (Figure 4.8) from which plot we determine the value of the tilt modulus. Then again as before, we study the variation in the tilt modulus for different values of $K_{long.,s}$ (Figure 4.9) and $K_{topo.}$ (Figure 4.10).

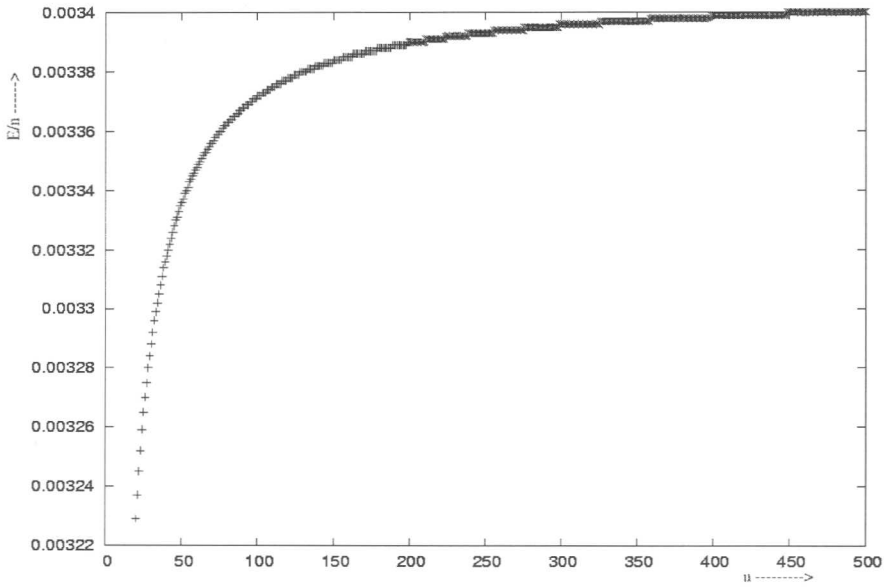

Figure 4.6: Energy values for different system sizes (tilt)

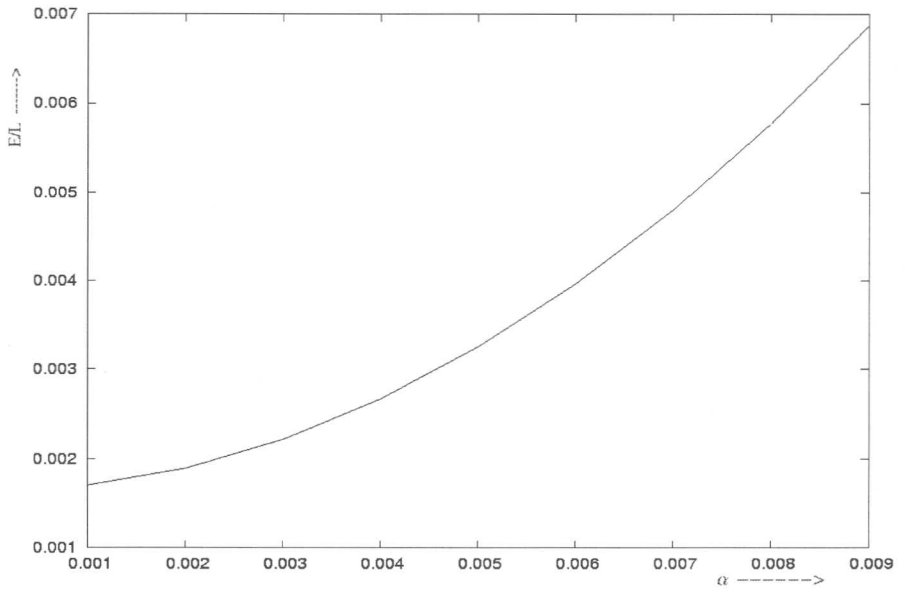

Figure 4.7: Energy/length for different tilt angles

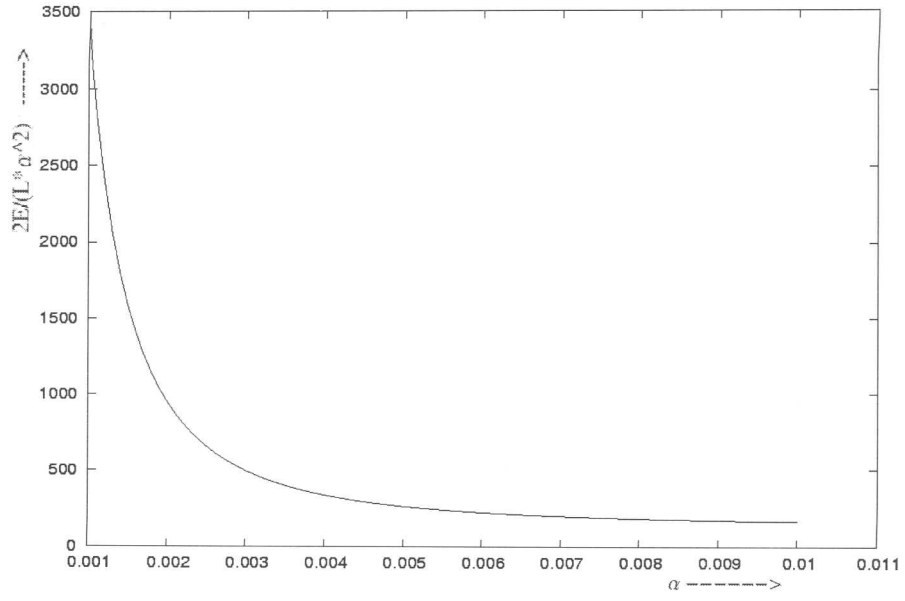

Figure 4.8: Energy/(L*τ^2) for different tilt angles

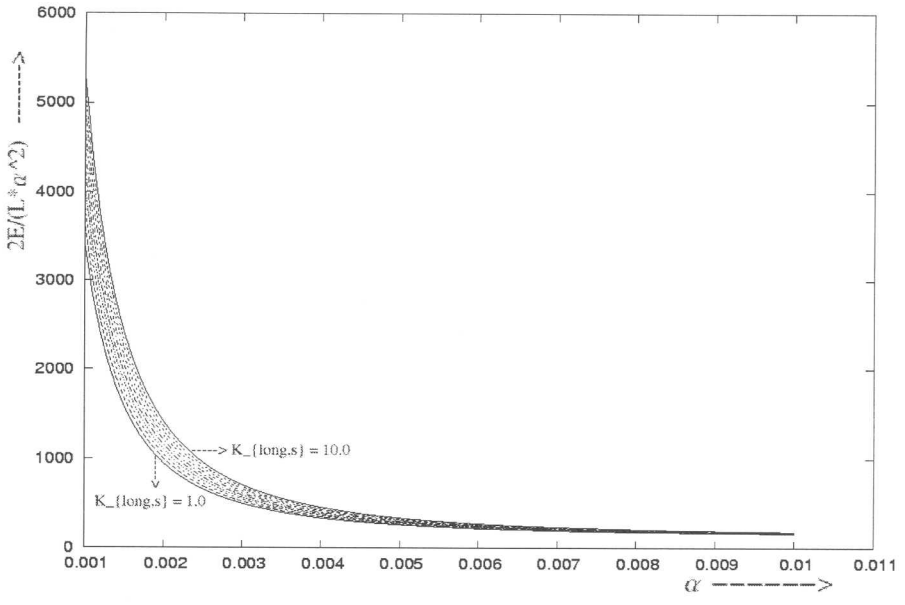

Figure 4.9: Energy/(L*τ^2) for different tilt angles at different $K_{long,s}$

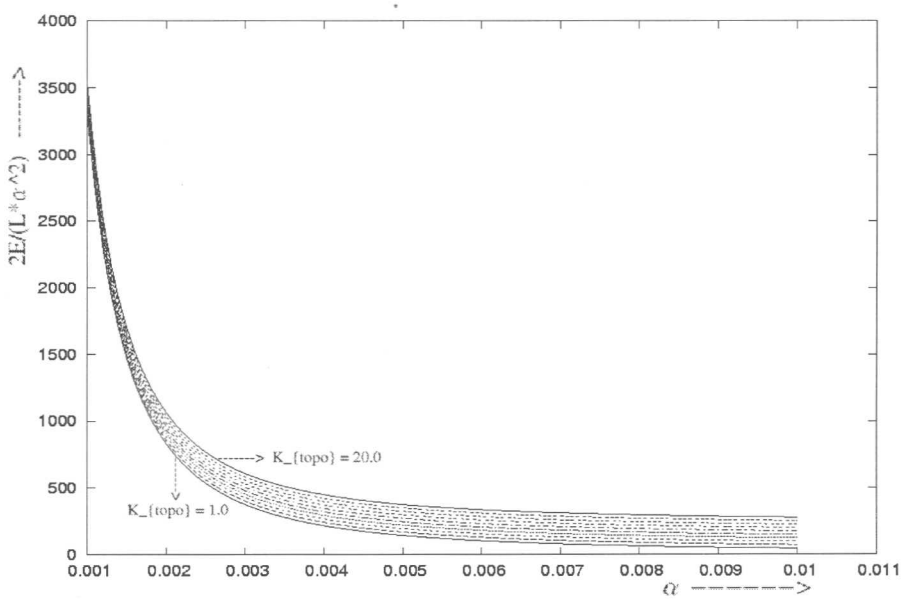

Figure 4.10: Energy/(L*τ^2) for different tilt angles at different K_{topo}

Chapter 5

ENERGY AND STRUCTURE IN DIFFERENT REGIMES

In this chapter, we shall look at the structures generated in different regimes of our model. The main results presented in this chapter are due to Monte-Carlo simulations. The results of Brownian Dynamics simulations are summarized in the last section.

5.1 Zero intrinsic curvature

5.1.1 Zero temperature, non-linear spring

Firstly, the microtubule was assumed to have a zero intrinsic curvature along the longitudinal direction. The bonds in the horizontal direction, i.e. along any given ring were assumed to be connected by non-linear springs. Then a zero temperature Monte-Carlo was carried out to generate the equilibrium structure. The initial configuration was a straight tube with all atoms at their equilibrium positions. As expected, the energy stayed at its minimum value (Figure 5.1) and the resultant structure was a straight undistorted tube (Figure 5.2).

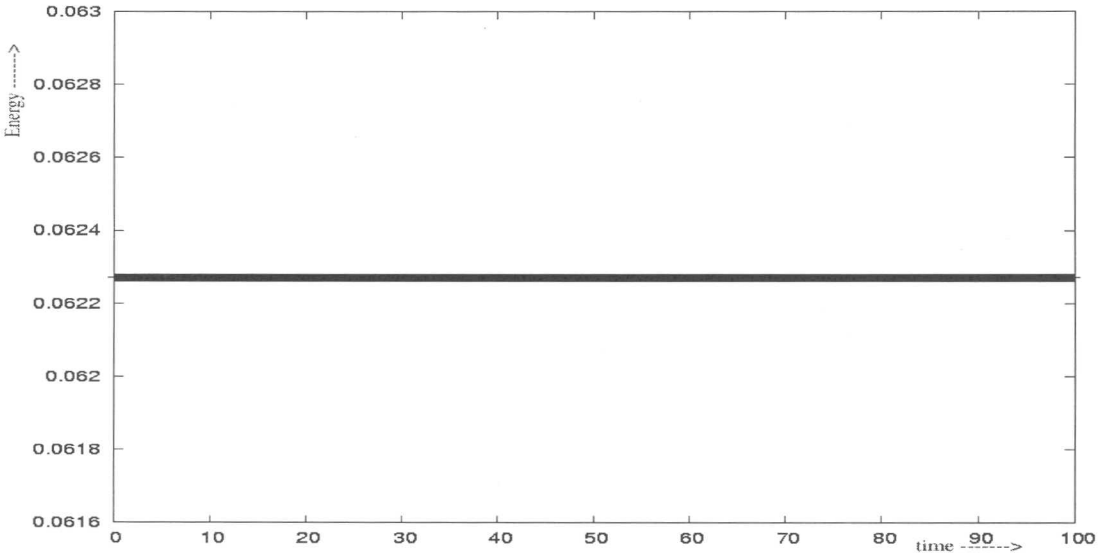

Figure 5.1: Energy vs time plot (Zero temp., zero curv., non-linear spring)

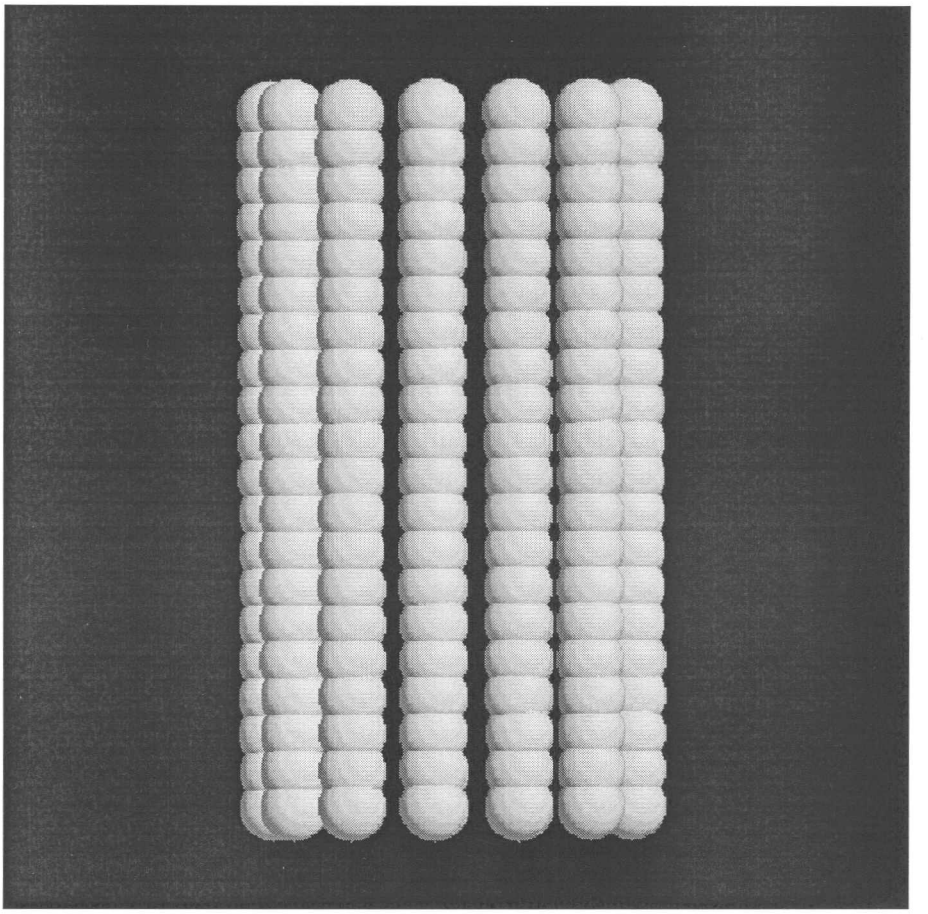

Figure 5.2: The structure of the MT (Zero temp., zero curv., non-linear spring)

5.1.2 Zero temperature, linear spring

Now, the microtubule was assumed to be connected along horizontal rings by linear bonds. The intrinsic curvature is again zero and the simulation is carried out at zero temperature. The initial configuration is the same as in the previous section and again, the energy plot remained constant (Figure 5.3) and the structure was a straight undistorted tube (Figure 5.4).

5.1.3 Finite temperature, non-linear spring

The MT is again assumed to have zero longitudinal curvature and the subunits on any given ring are assumed to be connected by non-linear springs. A Monte-Carlo simulation is carried out at finite temperatures and the equilibrium structure was generated. The initial configuration was a straight tube with all particles at their zero temperature equilibrium positions. The energy vs. time plot is shown (Figure 5.5) and the equilibrium structure was a fairly straight tube with some displacements due to the thermal noise (Figure 5.6).

5.1.4 Finite temperature, linear spring

As in the previous subsections, we again consider a MT with zero intrinsic curvature in the longitudinal direction. The horizontal springs are assumed to be linear and the system is allowed to relax at a finite temperature. The energy plot is generated (Figure 5.7) and the structure, as in the non-linear case, is an almost straight tube with slight displacements from the equilibrium position (Figure 5.8).

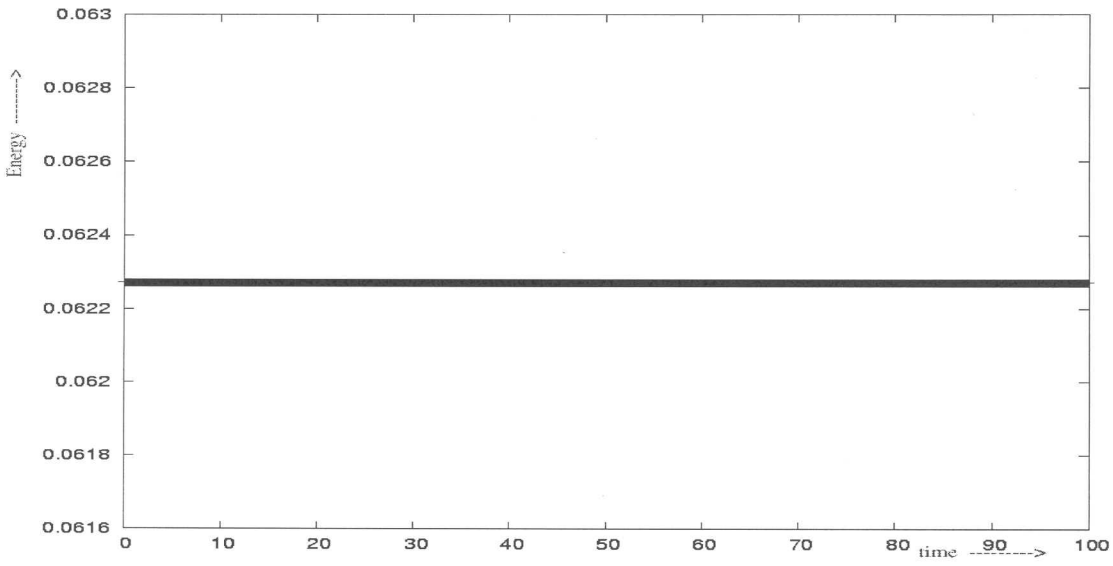

Figure 5.3: Energy vs time plot (Zero temp., zero curv., linear spring)

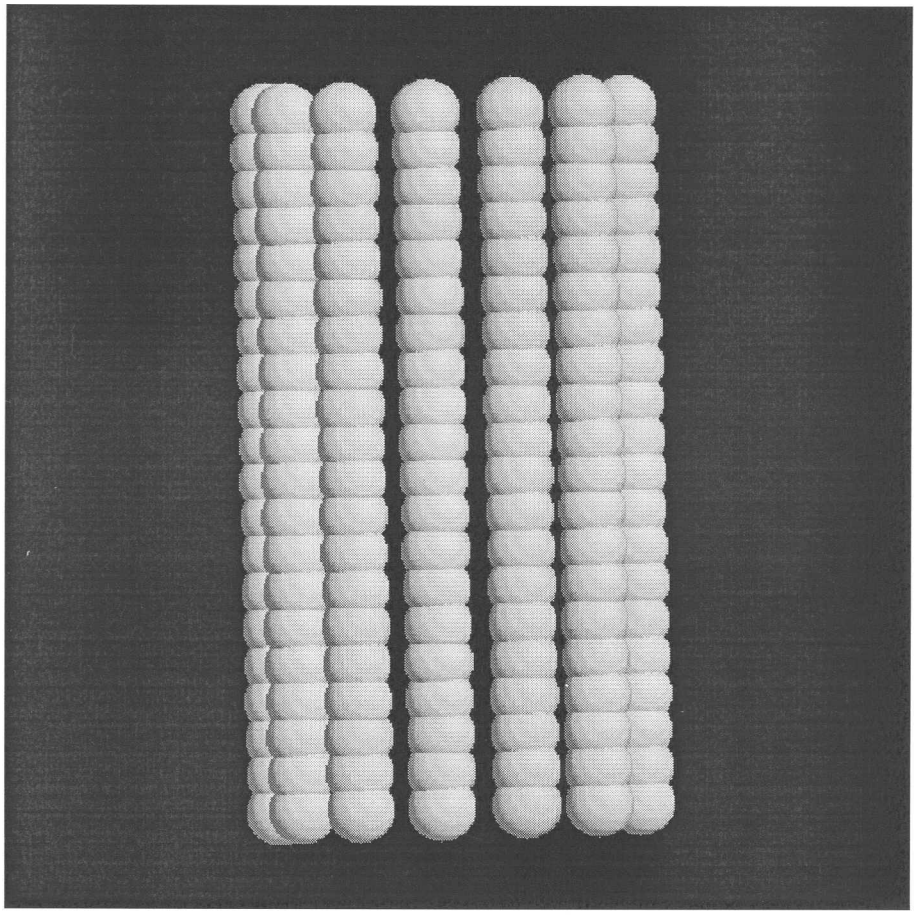

Figure 5.4: The structure of the MT (Zero temp., zero curv., linear spring)

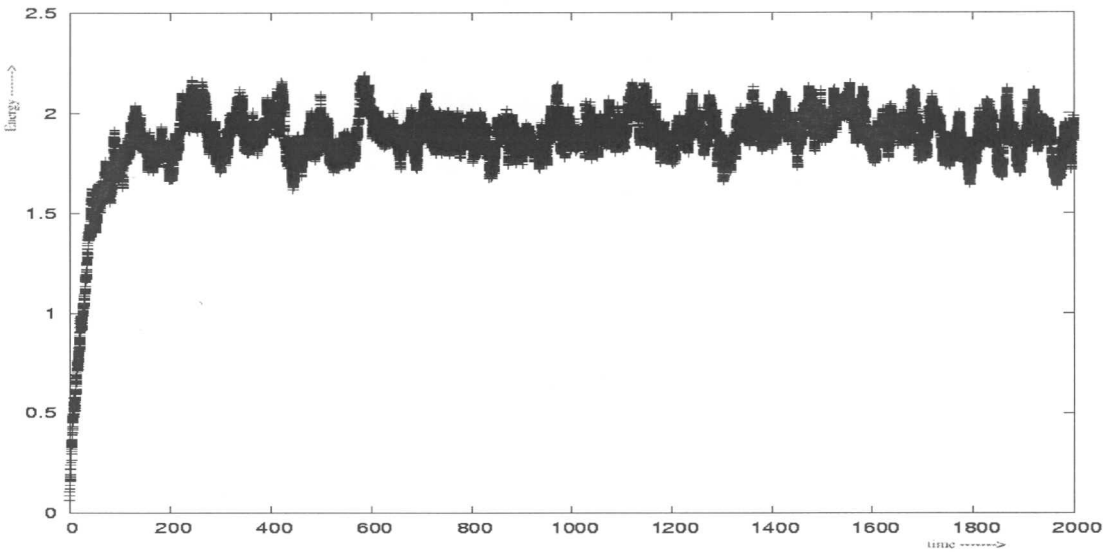

Figure 5.5: Energy vs time plot (Finite temp., zero curv., non-linear spring)

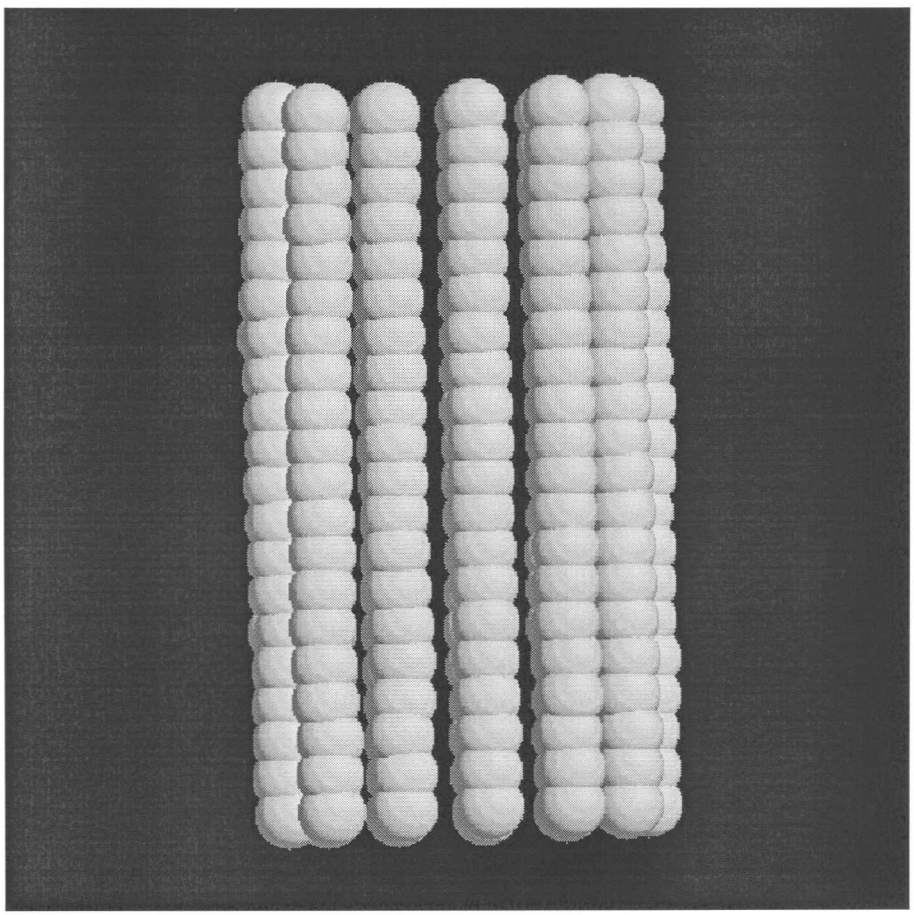

Figure 5.6: The structure of the MT (Finite temp., zero curv., non-linear spring)

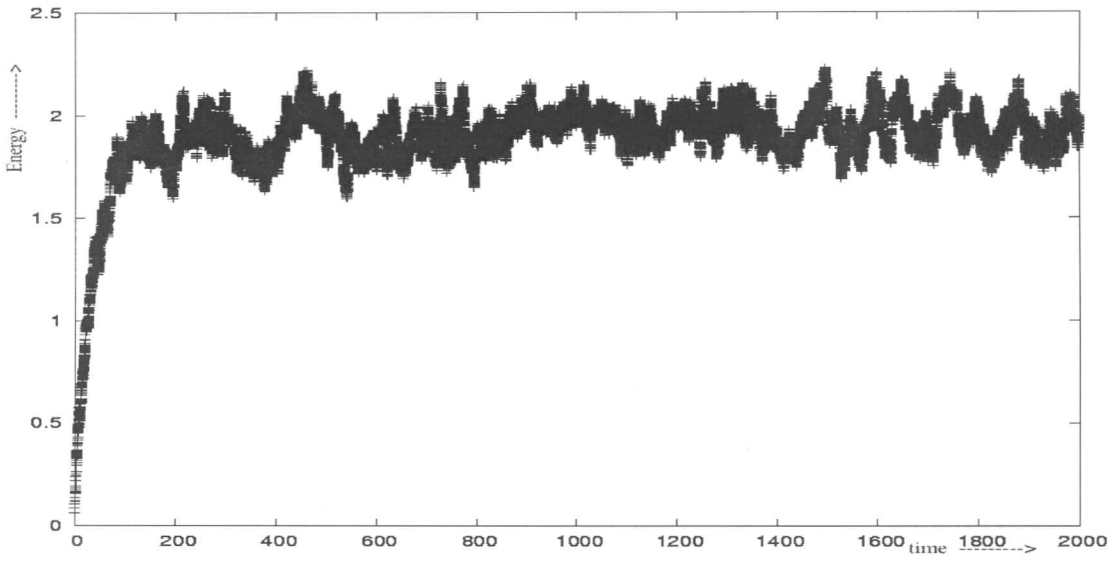

Figure 5.7: Energy vs time plot (Finite temp., zero curv., linear spring)

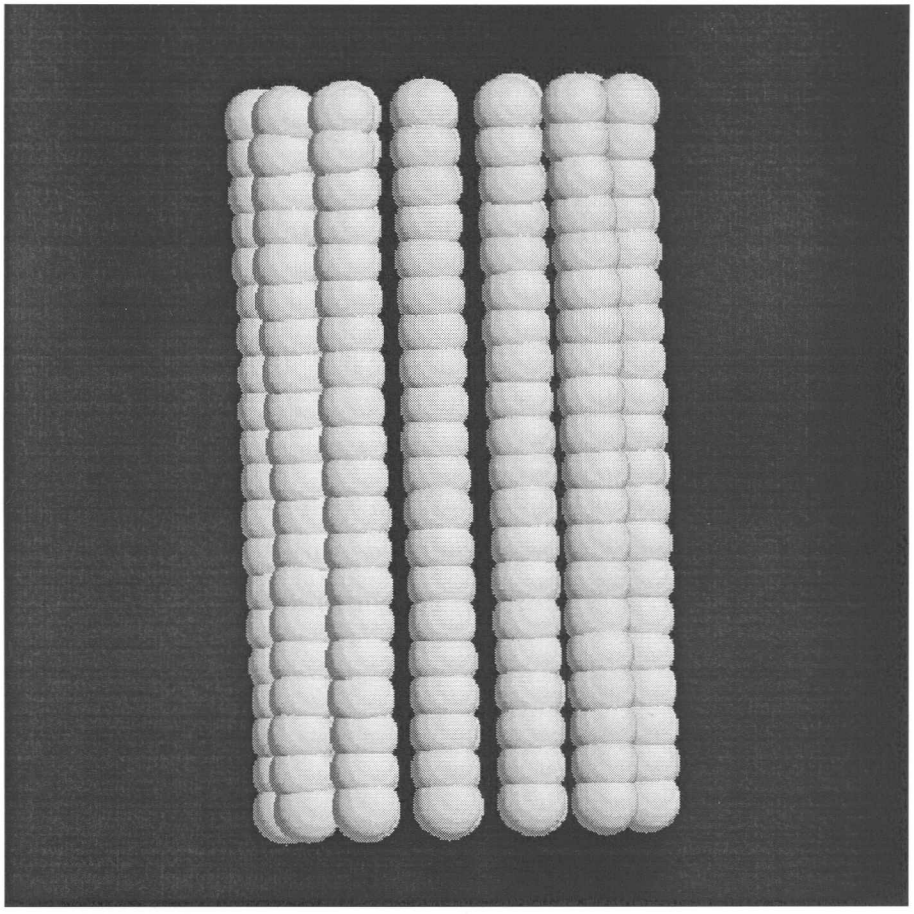

Figure 5.8: The structure of the MT (Finite temp., zero curv., linear spring)

5.2 Non-zero intrinsic curvature

5.2.1 Zero temperature, non-linear spring

Let us now consider a microtubule lattice that has a non-zero intrinsic curvature in the longitudinal direction, i.e. the bond angle between two successive bonds prefers to have a certain non-zero value. We assume that the horizontal bonds are connected by a non linear spring. We now allow the lattice to relax to its minimum energy configuration at zero temperature. The resultant graph is shown (Figure 5.9) and the structure that results (Figure 5.10) is a compromise between the two opposing curvatures. This competition is expected to manifest itself near the free end of the tube. Indeed, the structure obtain does in fact show that the structure near the ends is different from that in the bulk of the tube but the desired "flowering out" of the protofilaments could not be observed. Rather, a zig-zag pattern emerged in the protofilaments, with adjacent units on a ring also preferring to be in an "in-out" position. This is because we sought by introducing non-linear springs to make it more favourable for the horizontal bonds to increase in length but that also allows for relaxing by adopting the zig-zag structure, which is what the results seem to indicate.

5.2.2 Zero temperature, linear spring

Now, we consider a tube with non-zero intrinsic curvature but with the horizontal bonds now connected by linear springs. We again allow the tube to relax to its minimum energy configuration at zero temperature. We find the energy plot (Figure 5.11) and the equilibrium structure (Figure 5.12), as in the non-linear case, consists of a zig-zag pattern of tubulin near the free end of the MT. The linear spring implies that within the non-zero curvature, bending in towards the axis is equivalent in energy to bending outwards, thus producing the resultant structure.

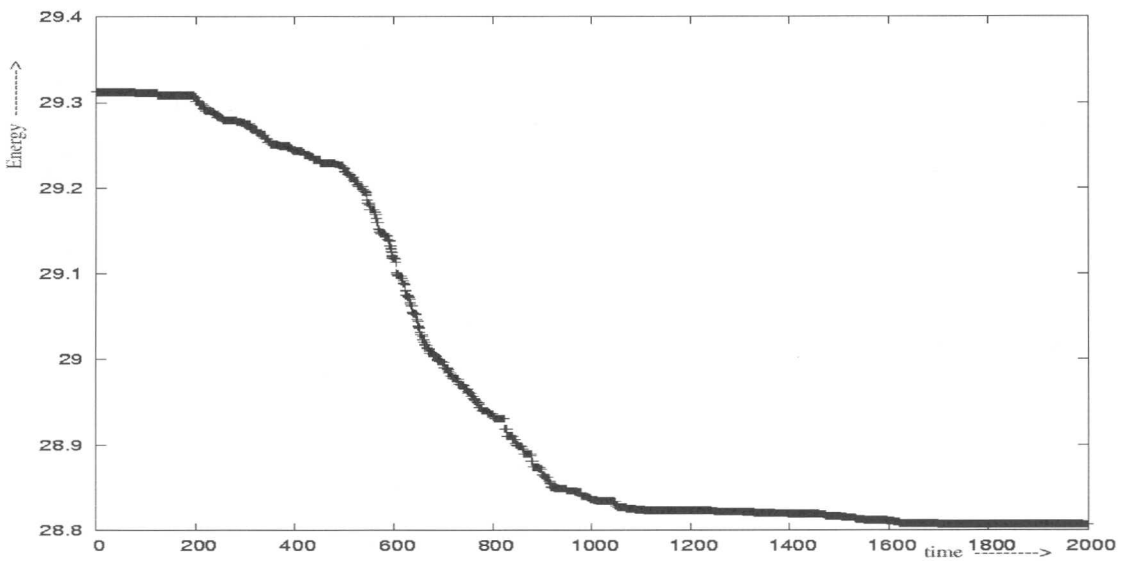

Figure 5.9: Energy vs time plot (Zero temp., non-zero curv., non-linear spring)

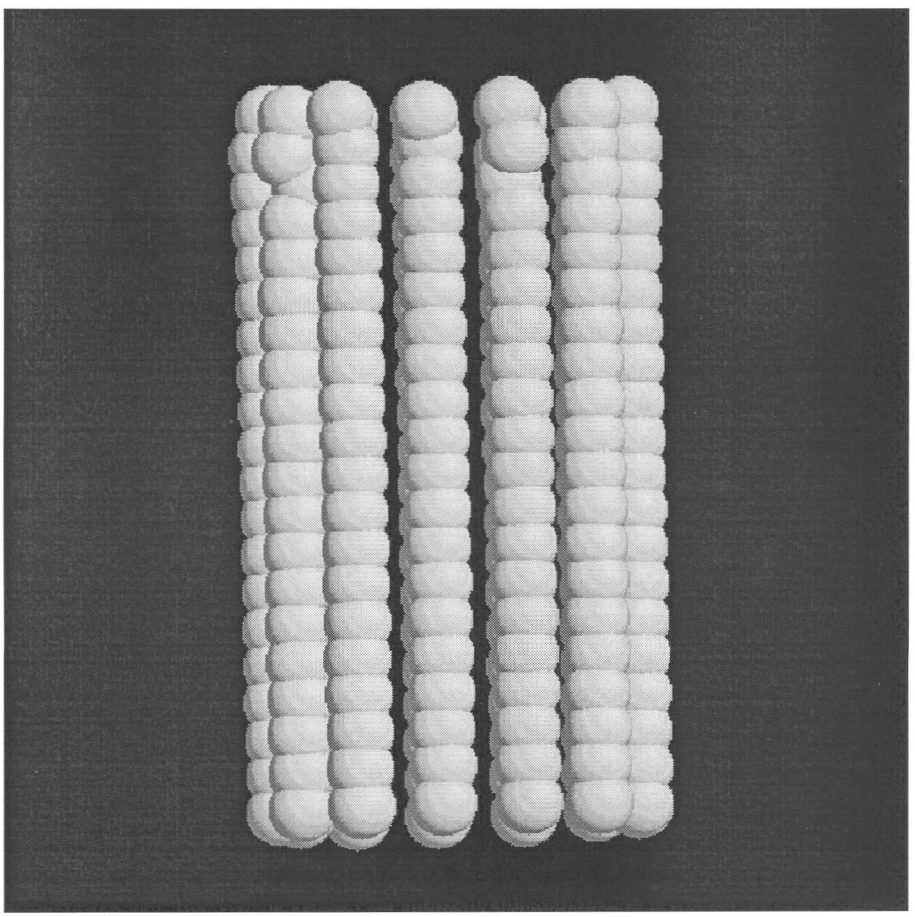

Figure 5.10: The structure of the MT (Zero temp., non-zero curv., non-linear spring)

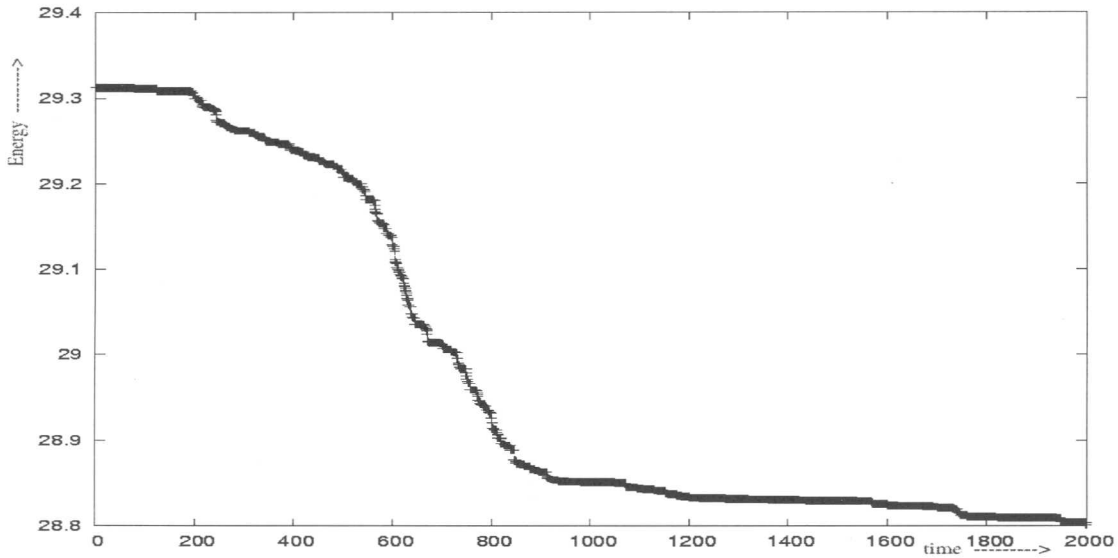

Figure 5.11: Energy vs time plot (Zero temp., non-zero curv., linear spring)

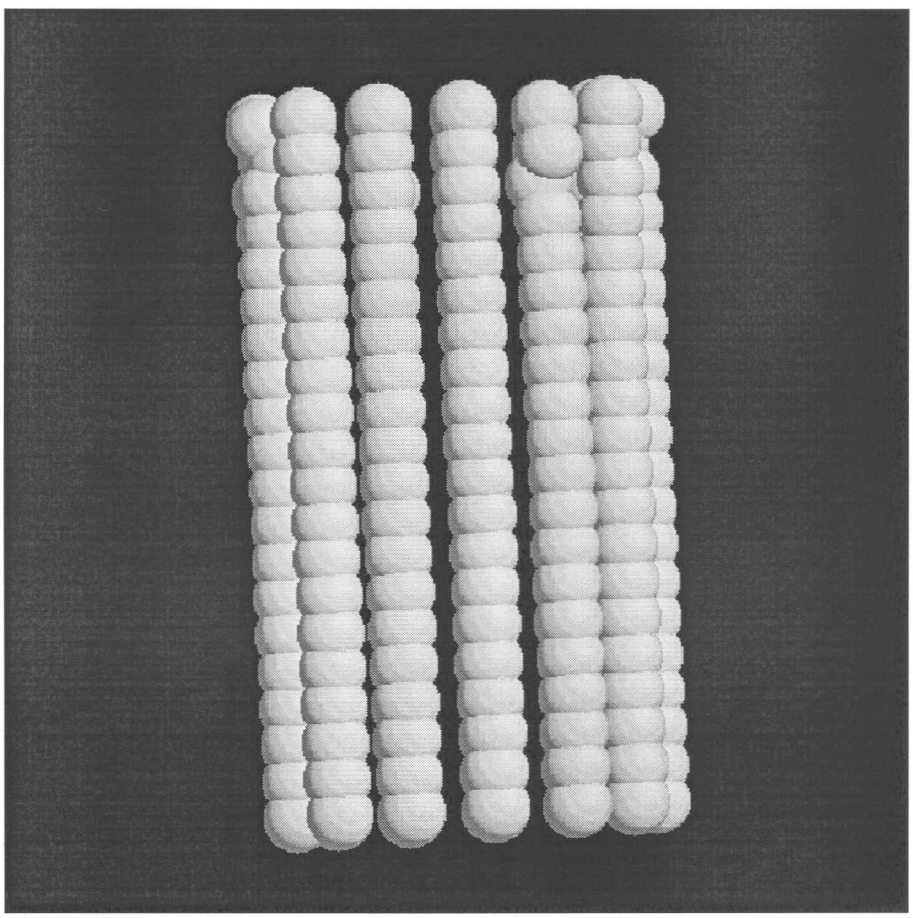

Figure 5.12: The structure of the MT (Zero temp., non-zero curv., linear spring)

5.2.3 Finite temperature, non-linear spring

We now consider a tube with a non-zero intrinsic curvature and with non-linear springs connecting the subunits in a ring and allow it to relax at a finite temperature. The energy curve is plotted (Figure 5.13) and the equilibrium structure is generated (Figure 5.14). The lattice shows considerable buckling throughout the length of the tube although angle variations are more pronounced near the ends of the tube.

5.2.4 Finite temperature, linear spring

Finally, we consider the case of the MT lattice with non-zero intrinsic curvature and with horizontal bonds connected through linear springs. Again a finite temperature Monte-Carlo was performed and the energy plot was obtained (Figure 5.15). The equilibrium structure (Figure 5.16) again shows a considerable distortion throughout the tube.

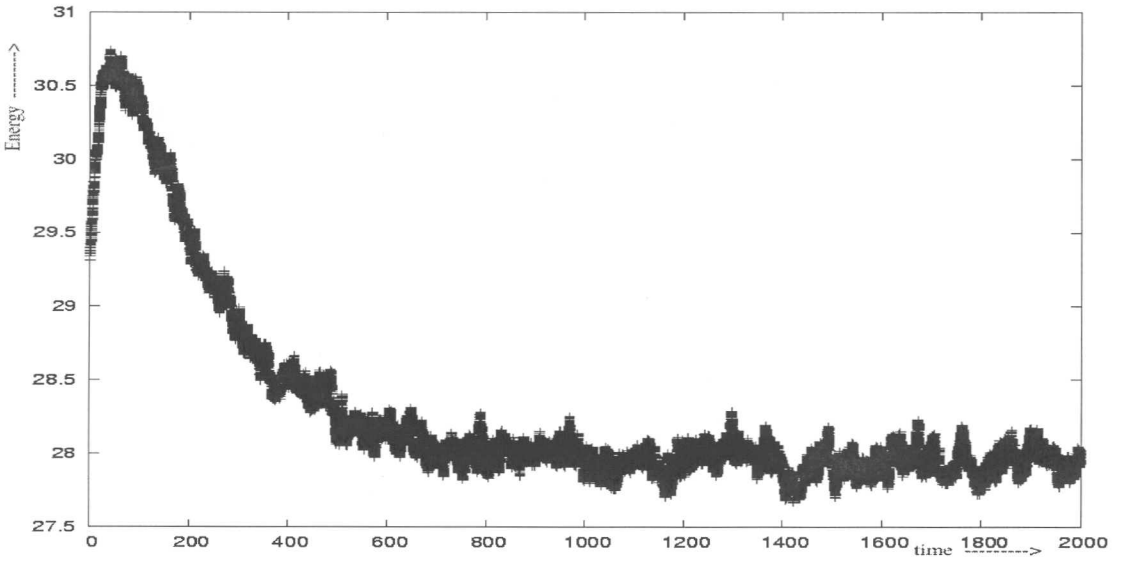

Figure 5.13: Energy vs time plot (Finite temp., non-zero curv., non-linear spring)

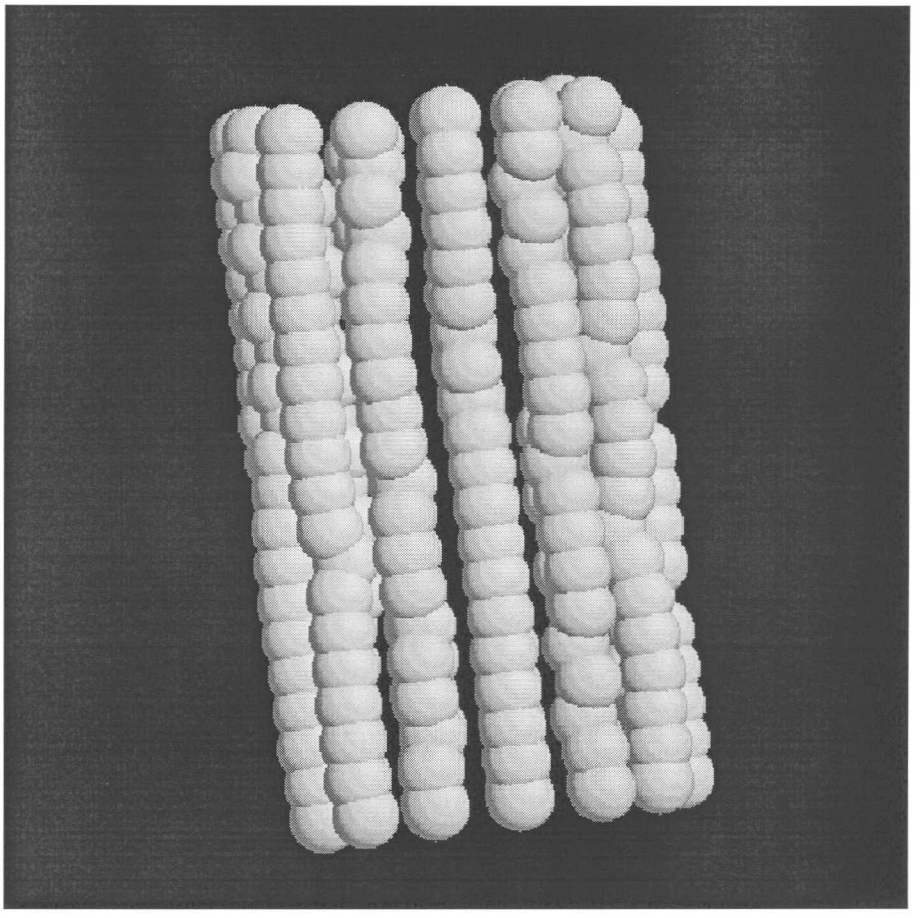

Figure 5.14: The structure of the MT (Finite temp., non-zero curv., non-linear spring)

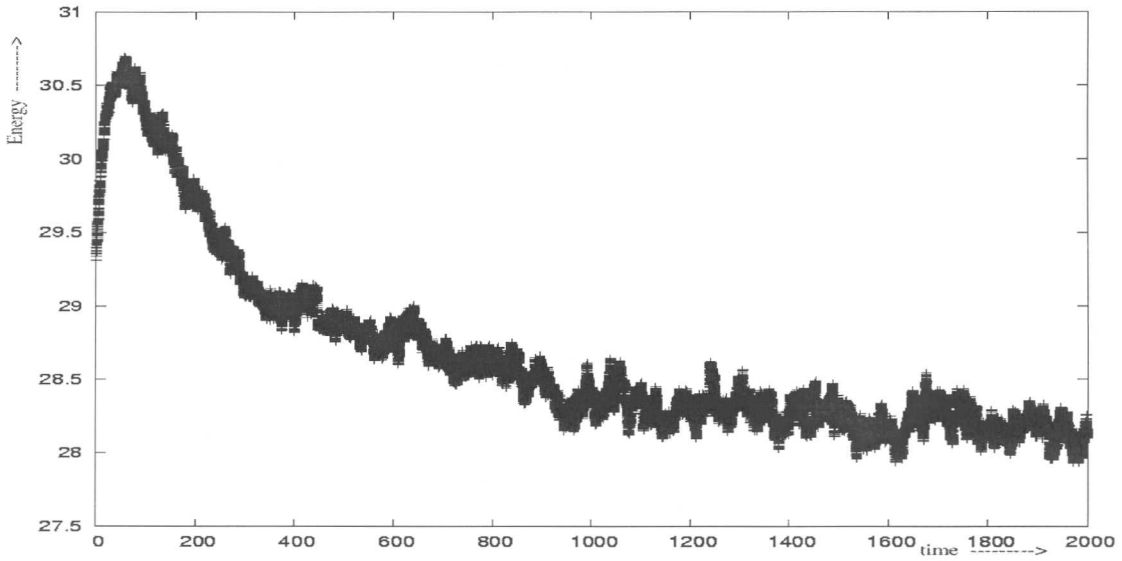

Figure 5.15: Energy vs time plot (Finite temp., non-zero curv., linear spring)

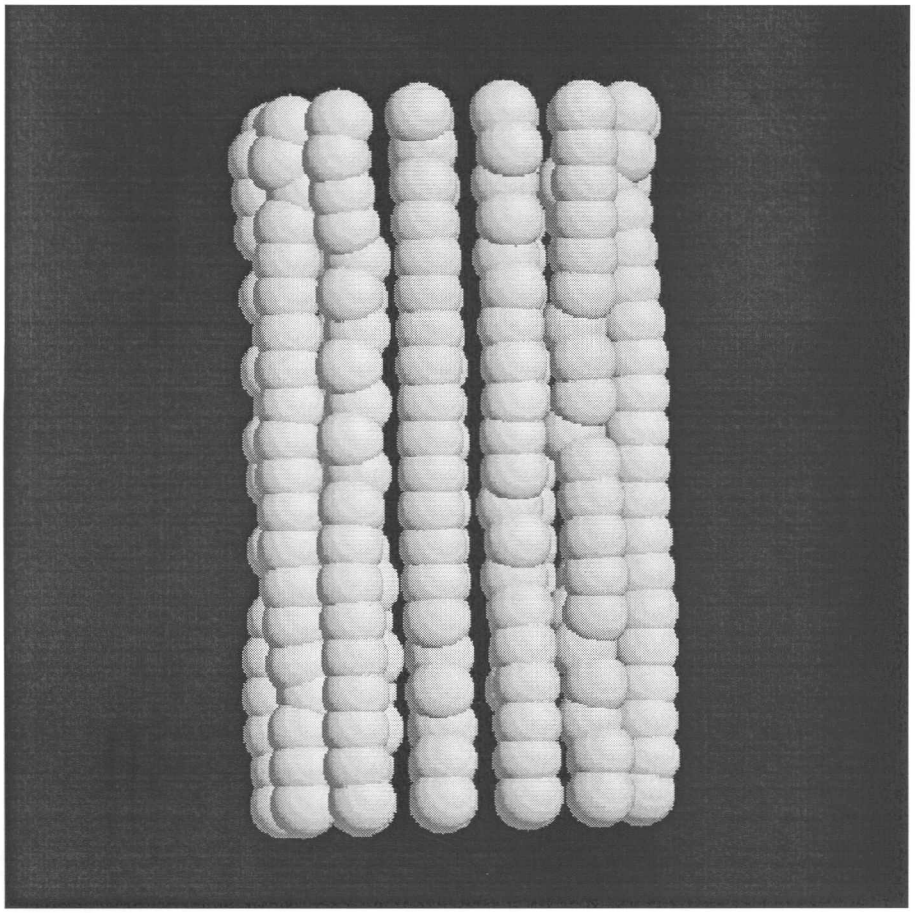

Figure 5.16: The structure of the MT (Finite temp., non-zero curv., linear spring)

5.3 Radius profiles

To obtain a feel for the structures that are generated by the above simulations, we trace the radius profile of the equilibrium structures that are obtained in the various cases. For the zero curvature case (Figure 5.17), while the zero temperature radii are perfectly constant, the finite temperature structures shows fluctuations on either side of the equilibrium positions.

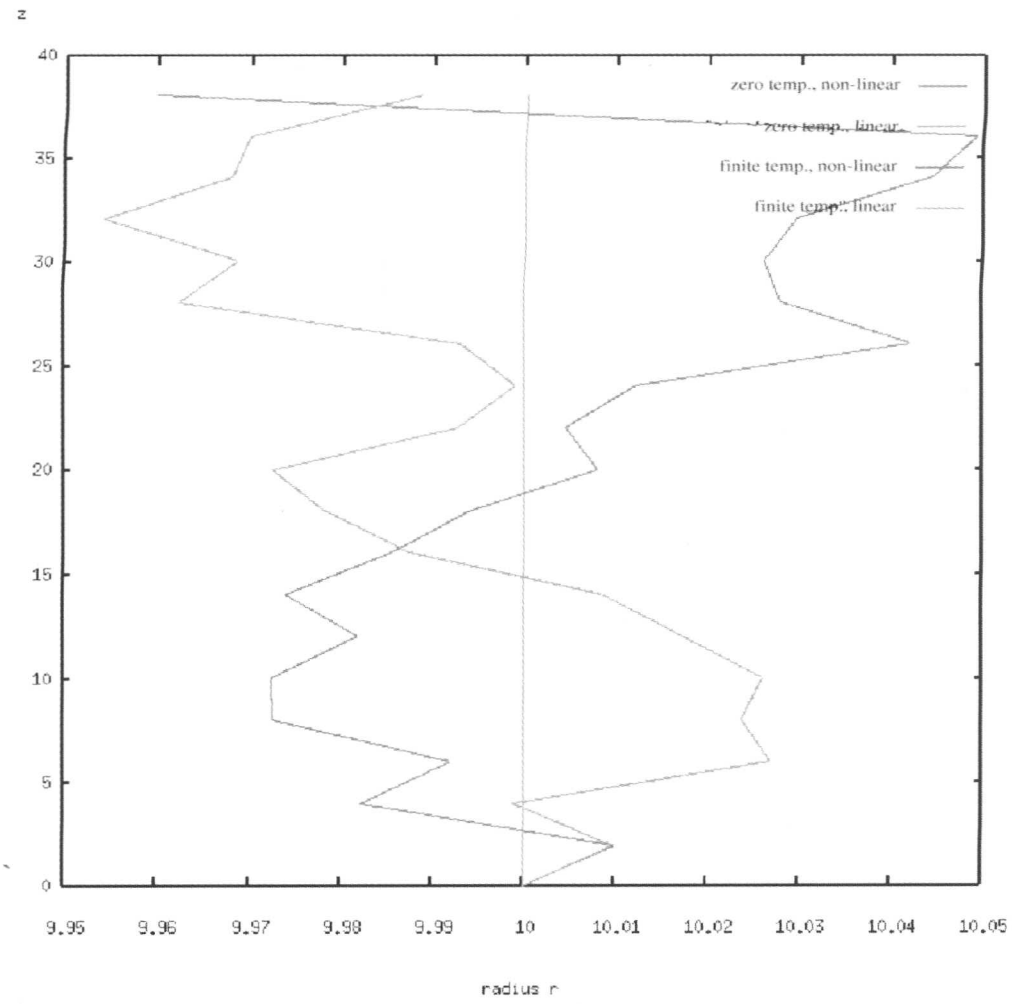

Figure 5.17: Radius profiles for the zero curvature structures

In the case of structures with non-zero longitudinal intrinsic curvature (figure 5.18), the radius profiles of the zero temperature configurations also deviate away from a perfect cylinder. For both the linear and the non-linear case, the distance from the central axis begins to change near the end of the tube in a zig-zag fashion, with the last ring being further away from the central axis. The finite temperature structures also display similar behaviours and additionally also displays fluctuations throughout the tube.

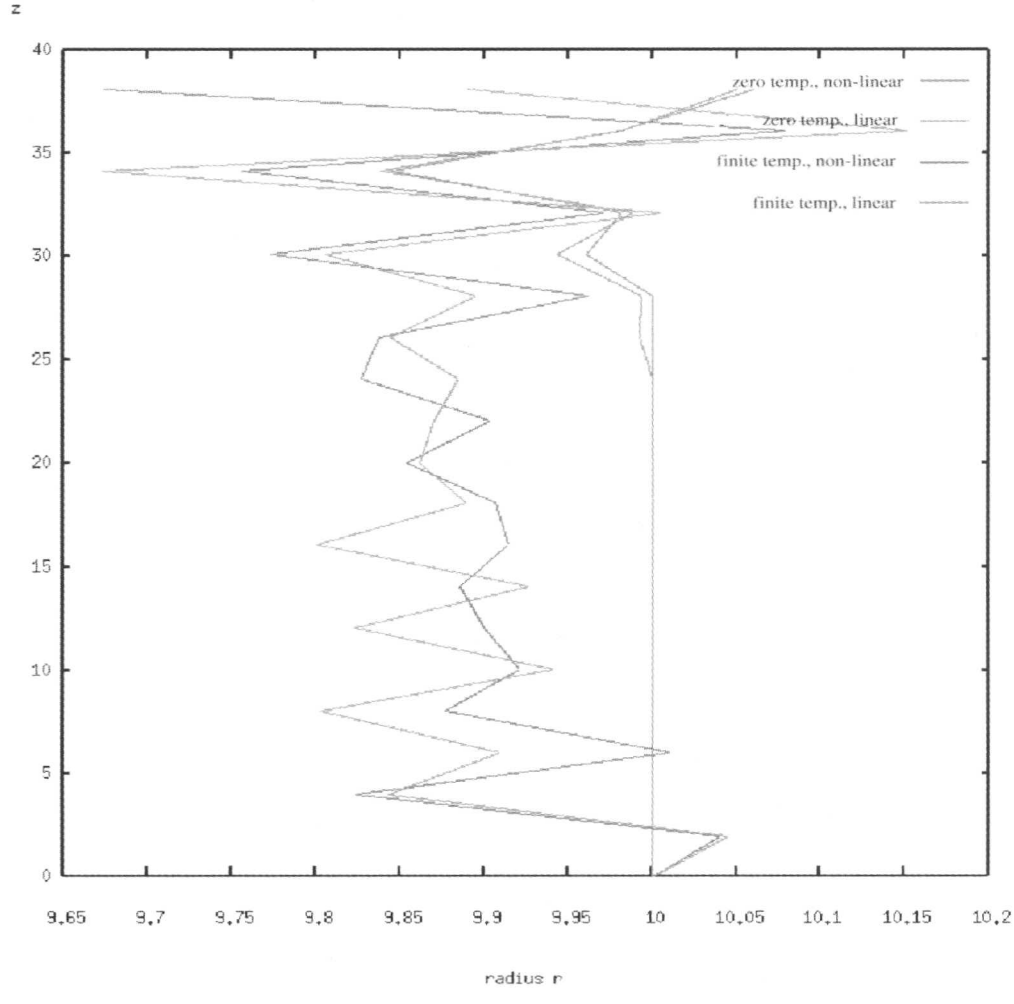

Figure 5.18: Radius profiles for the non-zero curvature structures

5.4 Curvature Energy costs

We also plot the curvature energy costs in the longitudinal direction. For the case of a tube with zero intrinsic curvature (Figure 5.19), the zero temperature energies are constant, while the finite temperature configurations show random fluctuations.

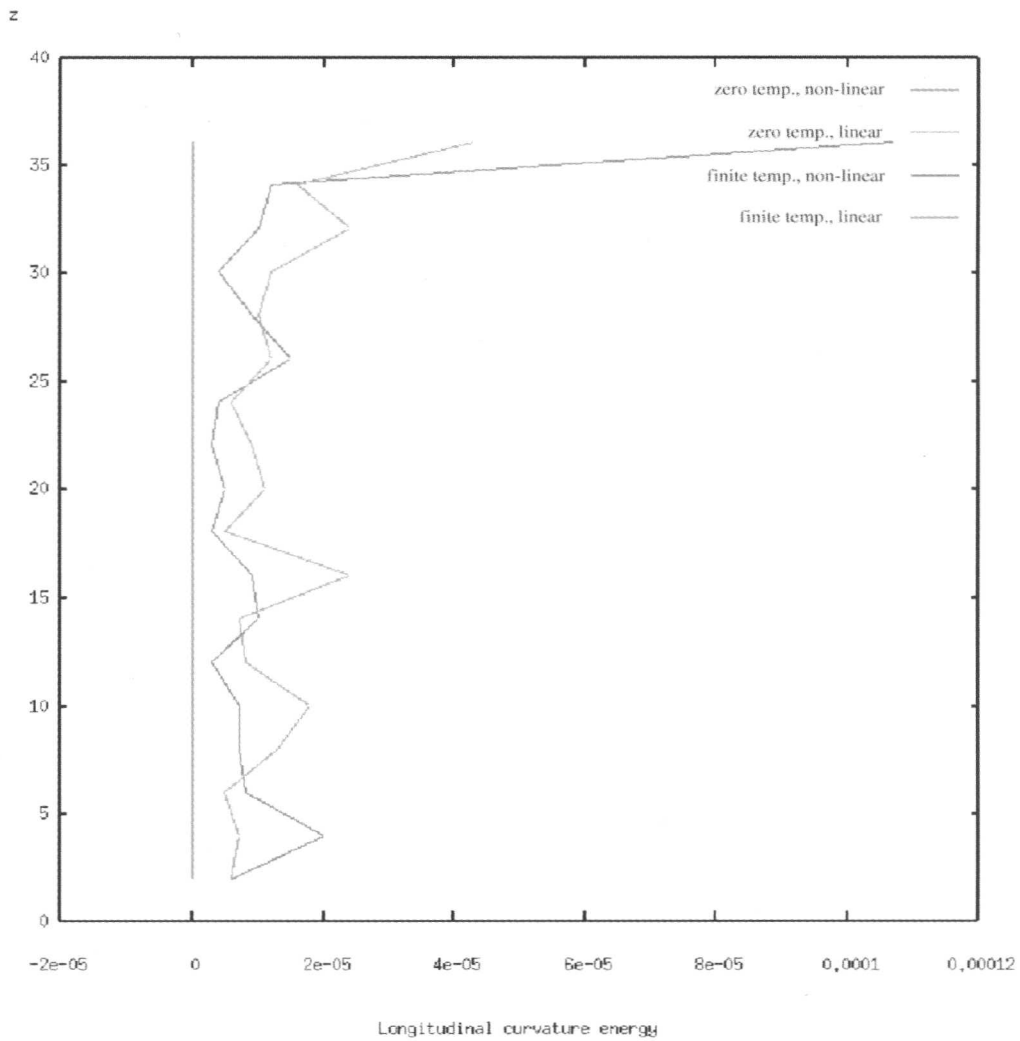

Figure 5.19: Curvature energy costs for zero curvature structures

For tubes with non-zero intrinsic curvatures (Figure 5.20), the zero temperature structures also lower their curvature energies by aligning themselves at suitable angles near the end of the tube. The finite temperature structures, as usual, show a similar behaviour near the ends and fluctuations throughout the tube.

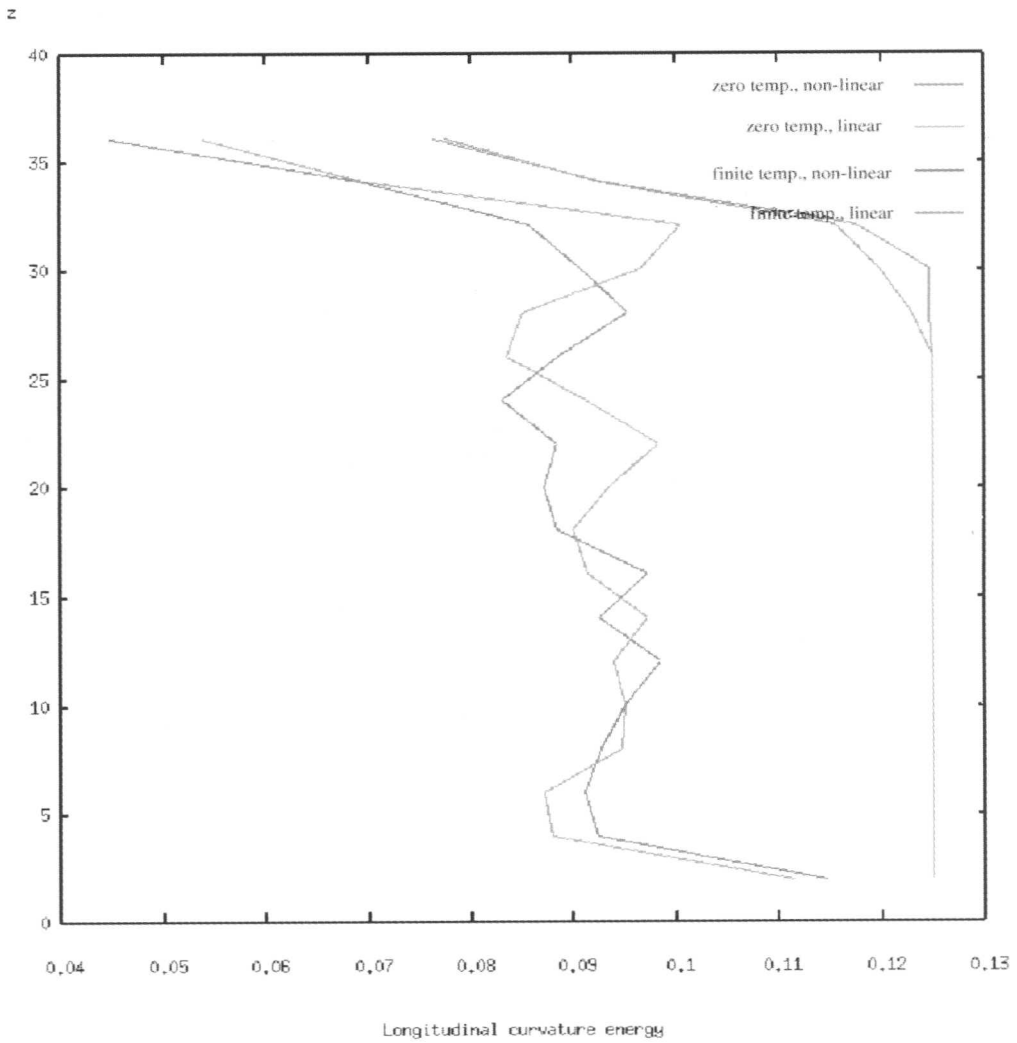

Figure 5.20: Curvature energy costs for non-zero curvature structures

5.5 Brownian Dynamics simulations

Brownian dynamics was also used to simulate the different regimes as mentioned in the earlier sections. For the case of a tube with zero intrinsic curvature, and at zero temperature, and with either linear or non-linear springs connecting the bonds in the lateral direction, for initial configuration of a perfectly straight tube, the energy plot, as in the Monte-Carlo case (Figures 5.1, 5.3), is a perfectly straight line and the resulting structure is a perfectly straight tube with all atoms at their individual equilibrium positions. Now for the case of a tube with zero intrinsic curvature taken at finite temperatures, for small values of the topology preserving spring constant, the energy plot stabilises at extremely high values of the energy, where all cylindrical structure is lost. An intermediate configuration shows that the cylinder starts twisting along its entire length (Figure 5.21), and then gradually collapses. It is conjectured that the twisted state of the tube represents a local energy minima, the barrier for getting out of which towards the actual minima is very high and may not achievable by a local algorithm such as Brownian Dynamics. However for large enough values of the spring constant $K_{topo.}$, the tube does stabilise (Figure 5.22) and results in a an almost straight configuration with some very small fluctuations (Figure 5.24).

For the case of the tube with a non-zero intrinsic curvature, even the zero temperature simulations escape into a region where the topology of the microtubule is not preserved. Again as before, we may stabilise the MT both at zero and finite temperatures (Figure 5.23) by increasing the topology preserving spring constant to a high enough value. The structures obtained are similar to Figure 5.24 in that they are almost straight.

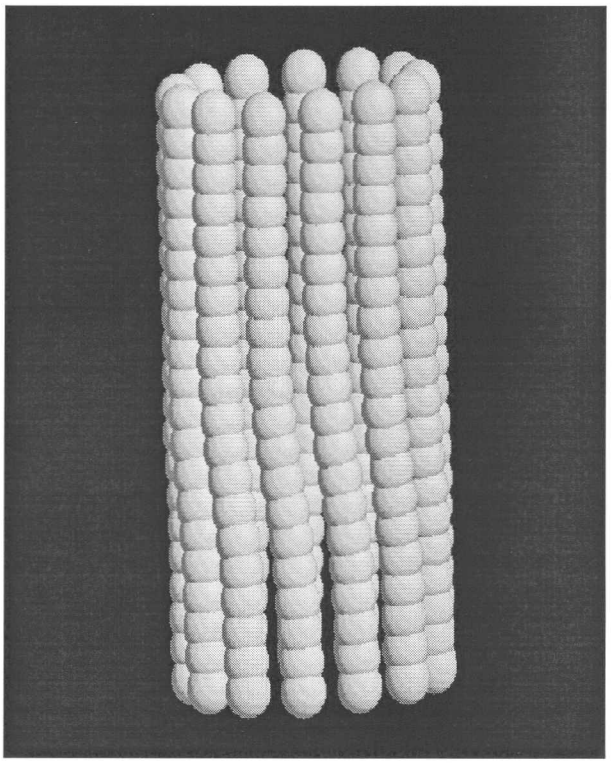

Figure 5.21: A view of a twisted intermediate structure before the MT collapses when the value of $K_{topo.}$ is small (zero curvature)

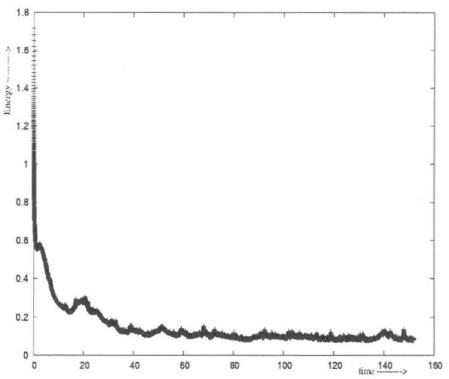

Figure 5.22: Energy plot for a high value of $K_{topo.}$ (zero curvature)

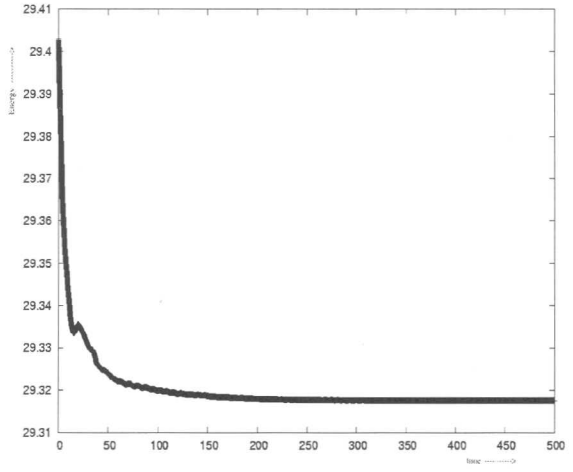

Zero temperature

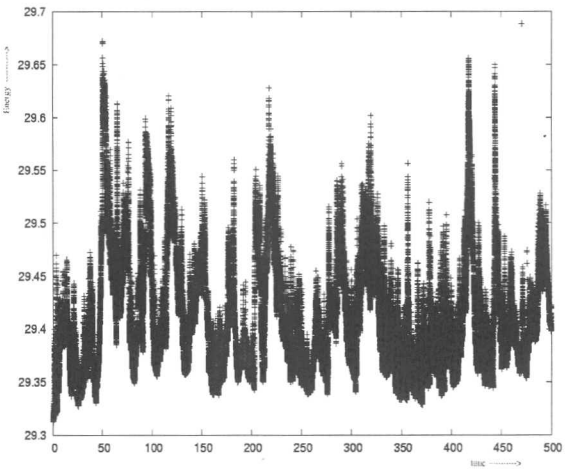

Finite temperature

Figure 5.23: Energy plots for non-zero curvatures

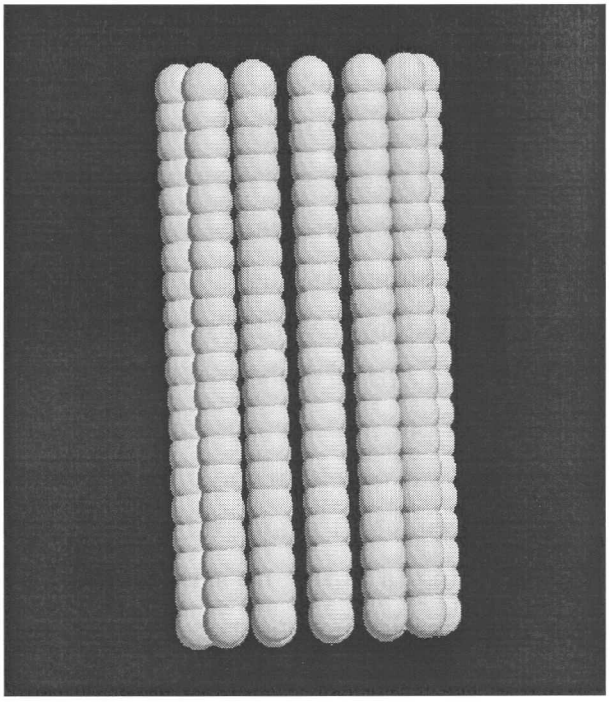

Figure 5.24: Final structure for a high value of $K_{topo.}$ (zero curvature)

Chapter 6

CONCLUSIONS AND FUTURE DIRECTIONS

In this thesis, we have developed a model for the microtubule that seeks to predict equilibrium structures based on microscopic interactions between the constituent tubulin heterodimers. We modelled the interactions based on expectations regarding the MT structure as known from experiments.

We have outlined a method and calculated the response of the microtubule lattice with zero intrinsic curvature and at zero temperature to small deformations about the equilibrium structure. In particular, the torsional and tilt moduli of the tube were calculated and their behaviour with changing model parameters (such as the various spring constants) were studied. We propose in the future to standardise the values obtained for the elastic moduli in this thesis with their experimentally determined values so that we can estimate the relationship of the values of various physical quantities obtained within our model to the actual physical values.

Central to the motivation for developing this microscopic model for microtubules was to generate the equilibrium structures that are observed experimentally. Specifically, one major aim is to see if a structural microtubule cap develops as a result of opposing curvatures of the microtubule lattice and to what extent it stabilises the MT. The simulation results of Chapter 5 indicate that our model gives sensible structures when the tube is intrinsically straight. However, as is seen from the results,

it is not yet clear how to enforce a non-zero longitudinal intrinsic curvature into our microscopic model. We hope to be able to find an efficient way to incorporate these opposing intrinsic curvatures into our model and then generate sensible equilibrium structures. With the help of the standardised model parameters, we can then find the actual energetics of the equilibrium structure and compare it to experiments.

Models such as these can be used to predict many aspects of microtubule dynamics which are currently inaccessible in experiments. Such models, although simplified, are powerful in that they can encapsulate the important contributions to the stability of the microtubule structure. In the future, we hope to develop microscopic models for microtubule dynamic instability as well as to investigate such interesting phenomena such as role of microtubule associated proteins and drugs such as colchicine and taxol in selectively stabilising and destabilising microtubules.

Appendix 1

PARAMETER VALUES

Table 1.1: Value of various parameters used in the simulations

Parameter description	Notation	Value
Equilibrium radius of a ring	r_0	10.0
Equilibrium bond length for the lateral bond	l_0	4.786
Equilibrium bond length for the vertical bond	d_0	2.0
Equilibrium bond angle in lateral direction	θ	$\frac{2\pi}{13}$
Equilibrium bond angle in vertical direction	ϕ	0 (zero curv.) or $\frac{\pi}{3}$ (non-zero curv.)
Spring constant for lateral spring	$K_{lat.,s}$	1.0
Spring constants for longitudinal spring	$K^1_{long.,s}$ $K^2_{long.,s}$ (if NL) $K^3_{long.,s}$ (if NL)	1.0 1.0 1.0
Force constant for angular deviations in the lateral direction	$K_{lat.,b}$	1.0
Force constant for angular deviations in the longitudinal direction	$K_{long.,b}$	1.0
Force constant for self-avoiding potential	K_{SA}	1.0
Force constant for topology preserving force	$K_{topo.}$	10.0 50.0 (for stable BD)
Friction coefficient	Γ	2.0
Width of Gaussian distribution for finite temperature simulations	A	0.02

References

Alberts, B., Johnson, A., Lewis, J., Raff, M., Roberts, K., and Walter, P. (2002). *Molecular Biology of the Cell.* Garland Science, Taylor and Francis Group, 4^{th} edition.

Caplow, M. and Fee, L. (2003). Concerning the chemical nature of tubulin subunits that cap and stabilize microtubules. *Biochemistry*, 42:2122–2126.

Caplow, M., Ruhlen, R., and Shanks, J. (1994). The free energy for hydrolysis of a microtubule-bound nucleotide triphosphate is near zero: all of the free energy for hydrolysis is stored in the microtubule lattice. *The Journal Of Cell Biology*, 127:779–788.

Caplow, M. and Shanks, J. (1996). Evidence that a single monolayer tubulin-GTP cap is both necessary and sufficient to stabilze microtubules. *Molecular Biology of the Cell*, 7:663–675.

Chrétien, D., Fuller, S. D., and Karsenti, E. (1995). Structure of Growing Microtubule Ends: Two-Dimensional Sheets Close Into Tubes at Variable Rates. *The Journal Of Cell Biology*, 129(5):1311–1328.

Chrétien, D., Jánosi, I., Taveau, J.-C., and Flyvbjerg, H. (1999). Microtubule's Conformational Cap. *Cell Structure and Function*, 24:299–303.

Dogterom, M. and Leibler, S. (1993). Physical aspects of the growth and regulation of microtubule structures. *Physical Review Letters*, 70(9):1347–1350.

Flyvbjerg, H., Holy, T. E., and Leibler, S. (1996). Microtubule dynamics: Caps, catastrophes, and coupled hydrolysis. *Physical Review E*, 54(5):5538–5560.

Fygenson, D. K. (2001). A Unifying Hypothesis for the Conformational Change of Tubulin. http://www.physics.ucsb.edu/ deborah/pub/FygensonXXXpp.pdf.

Hyman, A. A., Chretien, D., Arnal, I., and Wade, R. (1995). Structural changes accompanying GTP hydrolysis in microtubules: information from a slowly hydrolyzable analogue guanylyl-(α, β)- methylene-diphosphonate. *The Journal Of Cell Biology*, 128:117–125.

Hyman, A. A. and Karsenti, E. (1996). Morphogenetic Properties of Microtubules and Mitotic Spindle Assembly. *Cell*, 84:401–410.

Jánosi, I. M., Chrétien, D., and Flyvbjerg, H. (1998). Modeling elastic properties of microtubule tip and walls. *European Biophysical Journal*, 27:501–513.

Jánosi, I. M., Chrétien, D., and Flyvbjerg, H. (2002). Structural Microtubule Cap: Stability, Catastrophe, Rescue, and Third State. *Biophysical Journal*, 83:1317–1330.

Landau, L. and Lifshitz, E. (1986). *Theory of Elasticity*, volume 7 of *Course of Theoretical Physics*. Butterworth Heinemann, 3^{rd} edition.

Lodish, H., Baltimore, D., Berk, A., Zipursky, S. L., Matsudaira, P., and Darnell, J. (1995). *Molecular Cell Biology*. Scientific American Books, 3^{rd} edition.

Mitchison, T. and Kirschner, M. (1984). Dynamic instability of microtubule growth. *Nature*, 312:237–242.

Panda, D., Miller, H., and Wilson, L. (2002). Determination of the size and chemical nature of the stabilizing 'cap' at microtubule ends using modulators of polymerization dynamics. *Biochemistry*, 41:1609–1617.

Plischke, M., Vernon, D., Joós, B., and Zhou, Z. (1999). Entropic rigidity of randomly diluted two- and three-dimensional networks. *Physical Review E*, 60(3):3129–3135.

Tran, P., Walker, R., and Salmon, E. (1997). A metastable intermediate state of microtubule dynamic instability that differs significantly between plus and minus ends. *The Journal Of Cell Biology*, 138:105–117.